nature immunology

# Infection-specific phosphorylation of glutamyl-prolyl tRNA synthetase induces antiviral immunity

Eun-Young Lee[1,12], Hyun-Cheol Lee[2,12], Hyun-Kwan Kim[1,2], Song Yee Jang[1], Seong-Jun Park[3], Yong-Hoon Kim[4], Jong Hwan Kim[5], Jungwon Hwang[1], Jae-Hoon Kim[2], Tae-Hwan Kim[2], Abul Arif[6], Seon-Young Kim[5], Young-Ki Choi[7], Cheolju Lee[3,8], Chul-Ho Lee[4], Jae U Jung[9], Paul L Fox[6], Sunghoon Kim[10], Jong-Soo Lee[2] & Myung Hee Kim[1,11]

**The mammalian cytoplasmic multi-tRNA synthetase complex (MSC) is a depot system that regulates non-translational cellular functions. Here we found that the MSC component glutamyl-prolyl-tRNA synthetase (EPRS) switched its function following viral infection and exhibited potent antiviral activity. Infection-specific phosphorylation of EPRS at Ser990 induced its dissociation from the MSC, after which it was guided to the antiviral signaling pathway, where it interacted with PCBP2, a negative regulator of mitochondrial antiviral signaling protein (MAVS) that is critical for antiviral immunity. This interaction blocked PCBP2-mediated ubiquitination of MAVS and ultimately suppressed viral replication. EPRS-haploid (*Eprs*$^{+/-}$) mice showed enhanced viremia and inflammation and delayed viral clearance. This stimulus-inducible activation of MAVS by EPRS suggests an unexpected role for the MSC as a regulator of immune responses to viral infection.**



Aminoacyl-tRNA synthetases (ARSs) are essential for the catalysis of aminoacylation and thereby ensure high-fidelity protein synthesis; thus, the catalytic domains of ARSs are highly conserved throughout the three kingdoms[1]. Cytoplasmic ARSs have undergone substantial changes during the evolution of higher eukaryotes, including the addition of new domains with unique structural characteristics that are neither part of the enzymatic core nor present in prokaryotic homologs. Notably, these appended regions are associated with a broad range of biological functions; thus, ARSs have emerged as a new class of regulatory proteins with roles beyond protein synthesis. The activity of many ARSs in higher eukaryotes appears to be regulated by their presence in a cytoplasmic depot system called the 'MSC', which is assembled in most cases via the appended domains and consists of eight tRNA synthetases, including EPRS, and three auxiliary ARS-interacting multifunctional proteins AIMP1 (p43), AIMP2 (p38) and AIMP3 (p18)[2,3].

Under conditions of stress, several MSC components, including EPRS, methionyl-tRNA synthetase (MRS), lysyl-tRNA synthetase (KRS), AIMP1 and AIMP2, are released from the complex through post-translational modifications to exert activities during non-translational events such as inflammation[4], cell metabolism[5], angiogenesis[6] and tumorigenesis[7]. Phosphorylation is the critical regulatory mechanism that determines the non-translational function of ARSs in cells[8–10]. A representative example of this involves EPRS, the only bifunctional tRNA synthetase; EPRS comprises glutamyl-tRNA synthetase (ERS) and prolyl tRNA synthetase (PRS), which are coupled together via a linker containing three WHEP domains (named for a subset of synthetases (tryptophanyl-tRNA synthetase (W), histidyl-tRNA synthetase (H) and EPRS (EP)) with this domain). EPRS is thought to reside at the exterior of the MSC[11], consistent with its susceptibility to inducible release[9,12]. The residues Ser886 and Ser999 located between the ERS and PRS domains of EPRS are sequentially phosphorylated following stimulation by interferon-γ (IFN-γ), which promotes its dissociation from the MSC. Once EPRS escapes the MSC, it associates with nonstructural-protein-1-associated protein 1 (NSAP1), phosphorylated ribosomal protein L13a and glyceraldehyde-3-phosphate dehydrogenase (GAPDH) to form the IFN-γ-activated inhibitor of translation (GAIT) complex[13]. This regulatory complex binds to distinct 3′ untranslated regions (UTRs) of mRNAs that encode inflammatory proteins such as ceruloplasmin and thus suppresses their translation[3,4,14,15]. This specific function is thought to contribute to the resolution of chronic inflammation by controlling the expression of injurious pro-inflammatory molecules generated in response to the initial insults during infection[4]. We note that IFN-γ is produced in the context of an adaptive immune response during the late phase of infection and is secreted mainly by interleukin-12 (IL-12)-activated natural killer cells or type 1 helper T cells[16,17].

[1]Infection and Immunity Research Laboratory, Microbiomics and Immunity Research Center, Korea Research Institute of Bioscience and Biotechnology (KRIBB), Daejeon, Korea. [2]College of Veterinary Medicine, Chungnam National University, Daejeon, Korea. [3]Center for Theragnosis, Biomedical Research Institute, Korea Institute of Science and Technology, Seoul, Korea. [4]Laboratory Animal Resource Center, KRIBB, University of Science and Technology (UST), Daejeon, Korea. [5]Personalized Genomic Medicine Research Center, KRIBB, Daejeon, Korea. [6]Department of Cellular and Molecular Medicine, Lerner Research Institute, Cleveland Clinic, Cleveland, Ohio, USA. [7]College of Medicine and Medical Research Institute, Chungbuk National University, Cheongju, Korea. [8]Department of Biological Chemistry, UST, Daejeon, Korea. [9]Department of Molecular Microbiology and Immunology, Keck School of Medicine, University of Southern California, Los Angeles, California, USA. [10]Medicinal Bioconvergence Research Center, Department of Molecular Medicine and Biopharmaceutical Sciences, Graduate School of Convergence Science and Technology, Seoul National University, Seoul, Korea. [11]Biosystems and Bioengineering Program, UST, Daejeon, Korea. [12]These authors equally contributed to this work. Correspondence should be addressed to J.-S.L. (jongsool@cnu.ac.kr) or M.H.K. (mhk8@kribb.re.kr).

Received 4 June; accepted 28 July; published online 5 September 2016; doi:10.1038/ni.3542

The innate immune response is the first line of defense during the early phase of infection. Antiviral signaling is an essential cellular process that has evolved to respond to viral infection. Signaling is mainly mediated by RIG-I-like receptor (RLR) pathways, which include the key cytosolic sensors RIG-I and MDA5, which detect viral RNA[18]. These sensors subsequently interact with the central antiviral signaling protein MAVS, which in turn activates the transcription factors NF-κB and IRF3 via the cytosolic kinases IKK and TBK1, respectively; this cascade ultimately leads to induction of type I interferons and other antiviral molecules[18,19]. These signaling pathways are finely tuned by positive and negative regulatory mechanisms, which control antiviral responses through a complex network of proteins[20–22].

We hypothesized that the MSC, acting as a stimulus-dependent depot system, might be involved in the regulation of additional immune responses that specifically target viral infection. We found that one of the MSC components, EPRS, protected MAVS from its negative regulator PCBP2 ('poly(rC)-binding protein 2') via infection-specific modification and thereby facilitated the induction of antiviral innate immune responses. Thus, the MSC, which can respond rapidly to stress conditions without the need to activate gene transcription or protein synthesis, might also act as an immunoregulatory system directed against viral infection.

## RESULTS

### EPRS regulates immune responses to viral infection

ARSs have important roles in diverse non-translational cellular processes[1], but there is limited information about their role(s) during viral infection. Thus, we conducted a transcriptome analysis using RNA

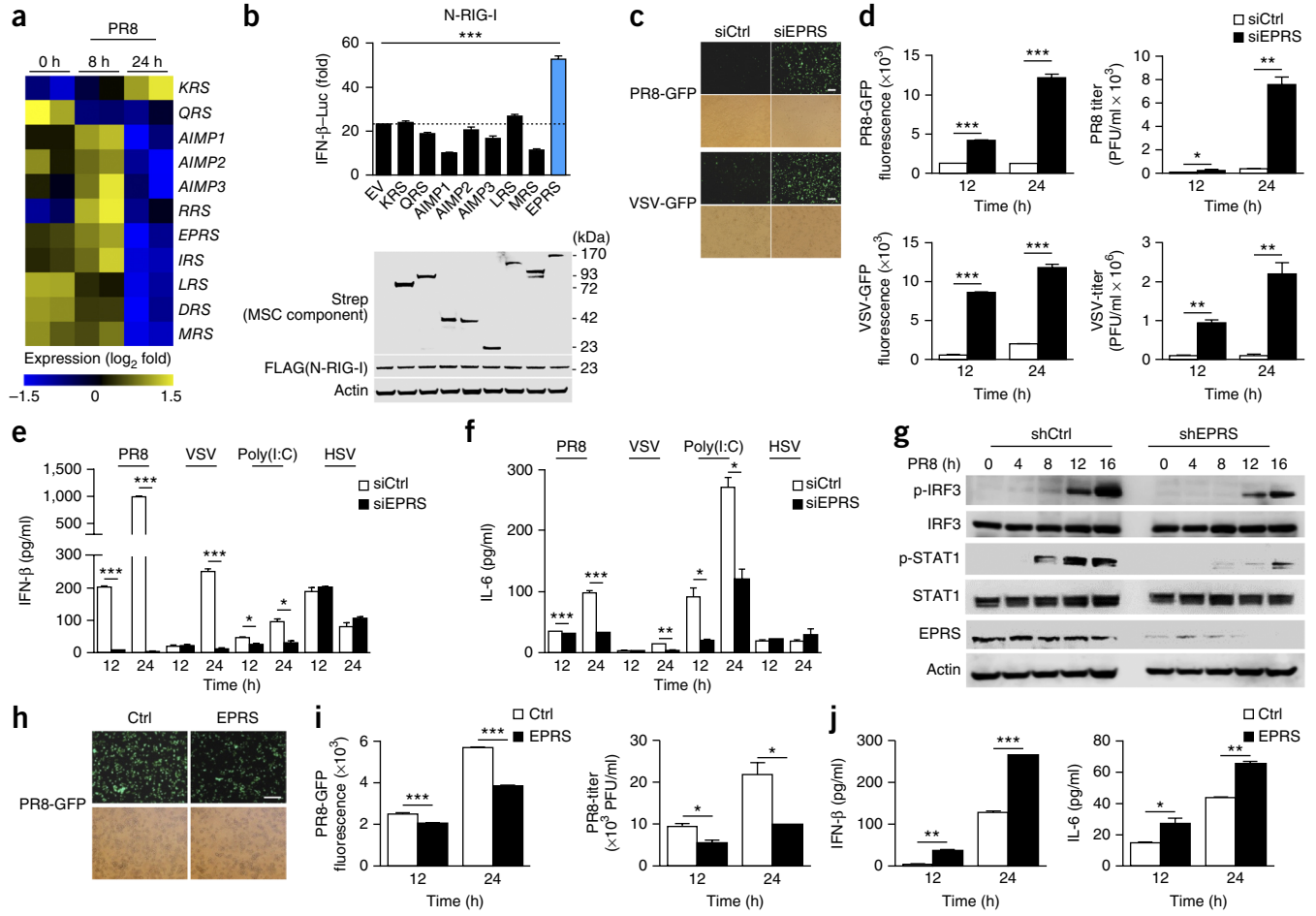


**Figure 1** EPRS induces antiviral immune responses to RNA viruses. (**a**) Expression of genes encoding MSC components (right margin) in bronchial epithelial cells (two replicates; one per column) at various times after infection with PR8 (above columns), showing genes upregulated (yellow) or downregulated (blue) over 1.5-fold relative to their expression before infection (key). (**b**) Luciferase activity of 293T cells transfected with the control TK-Renilla plasmid and a firefly luciferase reporter plasmid containing the *IFNB* promoter, plus empty vector (EV) or vector encoding various MSC components (horizontal axis), together with plasmid encoding the amino-terminal domain of RIG-I (N-RIG-I); results are presented relative to those of the renilla luciferase control. Below, immunoblot analysis of Strep-tagged MSC proteins and FLAG-tagged N-RIG-I in total lysates of the cells above. (**c**,**d**) Viral replication in RAW264.7 cells transfected with EPRS-specific siRNA (siEPRS) or control (non-targeting) siRNA (siCtrl) (key) and infected with PR8-GFP (multiplicity of infection (MOI) = 1) (top row) or VSV-GFP (MOI = 0.5) (bottom row), assessed by fluorescence microscopy (**c**) and fluorescence absorbance and plaque assay (**d**) at 24 h after infection. PFU, plaque-forming units. (**e**,**f**) Concentration of IFN-β (**e**) or IL-6 (**f**) in supernatants of RAW264.7 cells transfected with siRNA as in **c**,**d** (key) and infected with PR8-GFP, VSV-GFP or HSV-GFP (MOI = 1) or treated with poly(I:C) (80 μg) (above plots). (**g**) Immunoblot analysis of phosphorylated (p-) and total (inactive) IRF3 and STAT1, and of EPRS and actin (loading control), in PR8-GFP-infected RAW264.7 cells expressing EPRS-specific (shEPRS) or non-targeting control (shCtrl) short hairpin RNA. (**h**–**j**) Fluorescence microscopy (**h**), fluorescence absorbance and plaque assay (**i**), and secretion of IFN-β or IL-6 (**j**) of RAW264.7 cells transfected with empty vector (Ctrl) or vector encoding EPRS and infected with PR8-GFP. Scale bars (**c**,**h**), 100 μm. $*P < 0.05$, $**P < 0.01$ and $***P < 0.001$ (Student's *t*-test). Data are representative of one experiment (**a**) or three experiments with similar results (**b**–**j**), with at least three (**b**–**f**,**h**–**j**) or two (**g**) independent biological replicates (mean and s.d. of triplicates in **b**,**d**,**e**,**f**,**i**,**j**).

sequencing to assess the expression patterns of the genes encoding MSC components following infection of human bronchial epithelial cells with influenza A virus (PR8). We observed both heterogeneous expression and temporal fluctuation of these genes (**Fig. 1a**), which suggested a possible role for ARSs in responses to viral infection. We then assessed the ability of the MSC proteins to trigger antiviral responses and found that EPRS induced marked activity of the promoter of the gene encoding IFN-β (*IFNB*) (**Fig. 1b**). In addition, the expression of both EPRS mRNA and protein was slightly upregulated in multiple cell lines following viral infection (**Supplementary Fig. 1a**,**b**). Interferon-stimulated genes were also induced under the same conditions (**Supplementary Fig. 1c**). To evaluate whether induction of EPRS mRNA was caused by type I interferon, we treated human macrophage-like U937 cells and RAW264.7 mouse macrophages with IFN-β. Treatment with IFN-β resulted in substantial upregulation of expression of the ubiquitin-like protein ISG15 ('interferon-stimulated gene 15') but had little effect on the expression of EPRS mRNA (**Supplementary Fig. 1d**), which suggested that the *EPRS* gene was not controlled directly by interferon. No induction of EPRS mRNA was observed in cells depleted of RIG-I (**Supplementary Fig. 1e**), which indicated a requirement for sensing by the immune system in the induction of EPRS expression during infection with an RNA virus.

Small interfering RNA (siRNA)-mediated knockdown of EPRS in RAW264.7 cells (**Supplementary Fig. 2a**) increased the replication of RNA viruses (PR8 and vesicular stomatitis virus (VSV)) (**Fig. 1c**,**d**) but did not affect the replication of herpes simplex virus (HSV), a DNA virus (**Supplementary Fig. 2b**). Cells in which EPRS was knocked down showed considerable attenuation of the production of antiviral cytokines (IFN-β and IL-6) following viral infection or treatment with the synthetic double-stranded RNA poly(I:C) (**Fig. 1e**,**f**). HSV did not significantly alter cytokine induction (**Fig. 1e**,**f**). Similar results were obtained after viral infection of HEK293T human embryonic kidney cells in which EPRS was knocked down (**Supplementary Fig. 2c–e**) and RAW264.7 stably transduced with short hairpin RNA for knockdown of EPRS (**Supplementary Fig. 2f–l**). Furthermore, activation of the interferon-related signaling molecules IRF3 and STAT1 was significantly lower in cells in which EPRS was knocked down than in their EPRS-sufficient counterparts (**Fig. 1g**). In contrast, RAW264.7 cells stably overexpressing EPRS (**Supplementary Fig. 2m**) showed significantly less viral replication and more production of IFN-β and IL-6 following infection with PR8 (**Fig. 1h–j**) or VSV (**Supplementary Fig. 2n–p**) than those of their counterparts with basal expression of EPRS. Collectively, these data demonstrated that EPRS positively regulated antiviral innate immune responses, specifically those directed against RNA viruses.

### EPRS is critical for antiviral immunity *in vivo*

We used heterozygous $Eprs^{+/-}$ mice to investigate the physiological role of EPRS in antiviral immune responses *in vivo* because homozygous deletion of *Eprs* is lethal at the pre-weaning stage. We isolated bone-marrow-derived macrophages (BMDMs) from wild-type ($Eprs^{+/+}$) and $Eprs^{+/-}$ mice and infected the cells with PR8 or

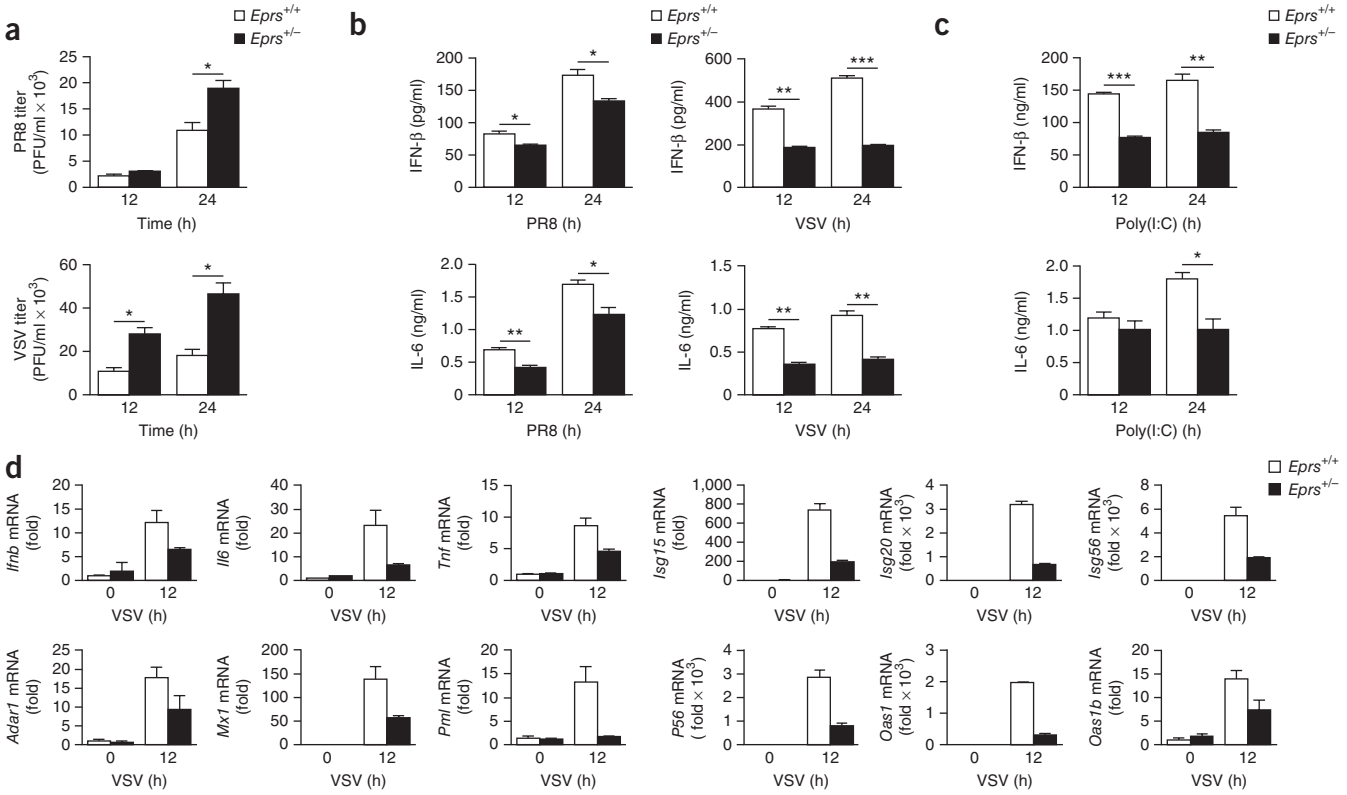


**Figure 2** EPRS is critical for antiviral defense against RNA viruses in mouse BMDMs. (**a**) Plaque assay of viral titers in $Eprs^{+/+}$ and $Eprs^{+/-}$ BMDMs infected with VSV-GFP (MOI = 5) (top) or PR8-GFP (MOI = 3) (bottom). (**b**,**c**) Concentration of IFN-β and IL-6 in culture supernatants of cell as as in **a** after viral infection as in **a** (**b**) or treatment with poly(I:C) (40 μg) (**c**). (**d**) Expression of *Ifnb*, *Il6* and other genes encoding interferon-related antiviral products (vertical axes) in $Eprs^{+/+}$ and $Eprs^{+/-}$ mouse-derived BMDMs at 12 h after infection with VSV-GFP. $^{*}P < 0.05$, $^{**}P < 0.01$ and $^{***}P < 0.001$ (Student's *t*-test). Data are representative three experiments with similar results, with three (**a**–**c**) or two (**d**) independent biological replicates (mean and s.d. of triplicates).

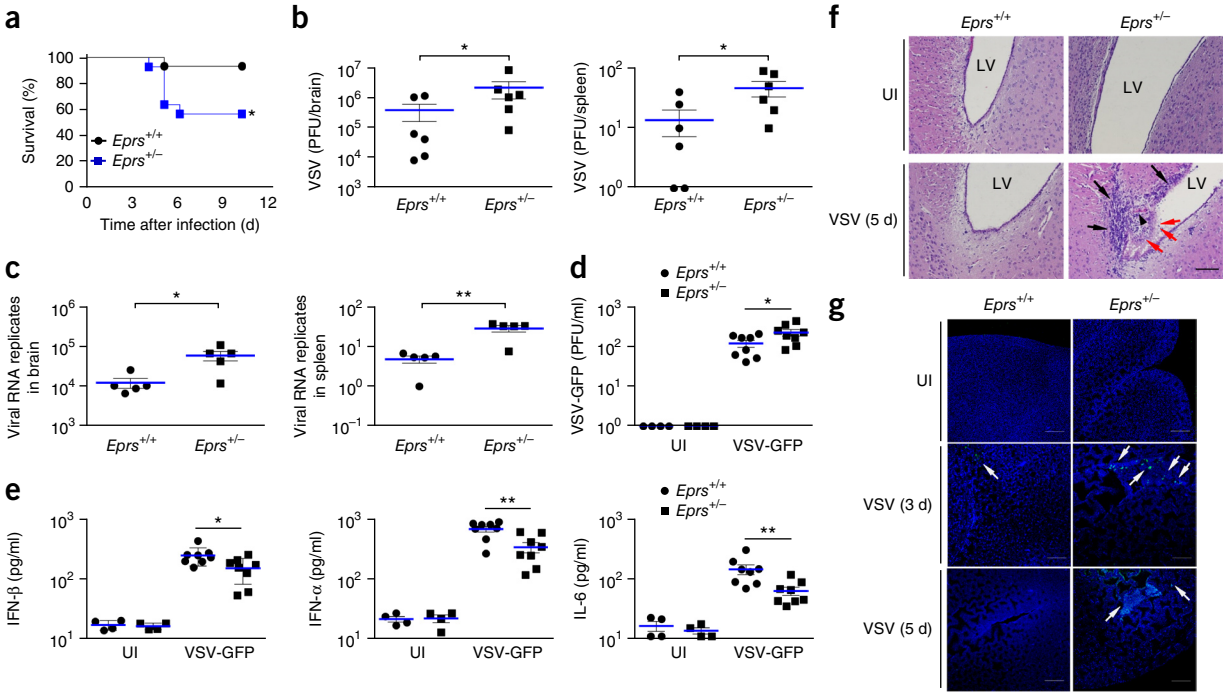


**Figure 3** EPRS is essential for antiviral immunity in mice. (**a**) Survival of 6- to 7-week-old female *Eprs*$^{+/+}$ mice ($n = 15$) and *Eprs*$^{+/-}$ mice ($n = 14$) monitored for 10 d after intravenous injection of VSV Indiana ($2 \times 10^8$ PFU per mouse). (**b**) Viral load in brain and spleen tissues of *Eprs*$^{+/+}$ and *Eprs*$^{+/-}$ mice ($n = 6$ per genotype), assessed by plaque assay at day 5 after infection as in **a**. (**c**) Viral loads in mice as in **b** ($n = 5$) determined by qPCR of VSV transcripts. (**d**,**e**) Plaque assay of viral load (**d**) and ELISA of IFN-β, IFN-α and IL-6 (**e**) in serum of *Eprs*$^{+/+}$ and *Eprs*$^{+/-}$ mice ($n = 8$ per genotype) left uninfected (UI) or at 12 h after infection with VSV-GFP ($2 \times 10^8$ PFU per mouse). (**f**) Hematoxylin-eosin-stained sections of brain tissue from *Eprs*$^{+/+}$ and *Eprs*$^{+/-}$ mice ($n = 4$ per genotype) left uninfected or on day 5 after mock infection or infection with VSV Indiana (left margin), showing well-preserved neural parenchyma (top and bottom left), or glial nodule formation by reactive microglial cells and mononuclear cells in brain parenchyma (black arrows), perivascular cuffing (arrowhead), and disruption of the ependymal lining (red arrows) at the lateral ventricle (LV), a result of massive infiltration of mononuclear cells (bottom right). (**g**) Immunohistochemical analysis, with anti-VSV-G, of brain sections from *Eprs*$^{+/+}$ and *Eprs*$^{+/-}$ mice ($n = 4$ per genotype) left uninfected or at days 3 and 5 after infection with VSV Indiana (left margin); nuclei were stained with DAPI; white arrows indicate VSV-positive GFP signals. Scale bars (**f**,**g**), 100 μm. $^*P < 0.05$ and $^{**}P < 0.01$ (log-rank test (**a**) or Mann-Whitney test (**b**–**e**)). Data are representative of one experiment (**a**) or three experiments with similar results (**b**–**g**), with two independent biological replicates (mean and s.e.m. in **b**–**e**).



VSV and found that the viral titer in *Eprs*$^{+/-}$ BMDMs was much higher than that in wild-type BMDMs (**Fig. 2a**). Consistent with that observation, the concentration of IFN-β and IL-6 produced by *Eprs*$^{+/-}$ BMDMs was significantly lower than that produced by *Eprs*$^{+/+}$ cells in response to both viral infection (**Fig. 2b**) and treatment with poly(I:C) (**Fig. 2c**). Similar results were obtained following siRNA-mediated knockdown of EPRS in mouse BMDMs (**Supplementary Fig. 3a–d**). Moreover, the expression of *Ifnb* and genes encoding antiviral interferon-related and inflammation-related products was much lower in VSV-infected *Eprs*$^{+/-}$ BMDMs than in their *Eprs*$^{+/+}$ counterparts (**Fig. 2d**). The induction of genes encoding antiviral products was also much lower following PR8 infection of RAW264.7 cells in which EPRS was knocked down than that in similarly infected cells in which EPRS was not knocked down (**Supplementary Fig. 3e**). In contrast, there was no substantial difference between HSV-infected *Eprs*$^{+/+}$ BMDMs and HSV-infected *Eprs*$^{+/-}$ BMDMs in their viral replication or cytokine secretion (**Supplementary Fig. 3f,g**).

Next, we challenged *Eprs*$^{+/+}$ and *Eprs*$^{+/-}$ mice intravenously with the VSV Indiana strain and monitored their survival daily. We found that 43% of *Eprs*$^{+/-}$ mice (6 of 14) but only 7% of *Eprs*$^{+/+}$ mice (1 of 15) died within 6 d of infection (**Fig. 3a**). To investigate the viral load in mouse tissue, we sampled and analyzed the brain and spleen of mice at day 5 after viral infection. Viral titers in the brain and spleen of *Eprs*$^{+/-}$ mice were significantly higher than in those of EPRS$^{+/+}$ mice (**Fig. 3b**,**c**), which indicated that *Eprs*$^{+/-}$ mice were more susceptible to VSV infection. To further assess the functional importance of EPRS during immune responses, we gave *Eprs*$^{+/+}$ and *Eprs*$^{+/-}$ mice intravenous injection of recombinant VSV expressing green fluorescent protein (GFP) and measured the viral load and expression of antiviral cytokines in serum samples 12 h after infection. Viremia was greater (**Fig. 3d**) and the concentration of IFN-β, IFN-α and IL-6 in the serum was lower (**Fig. 3e**) in *Eprs*$^{+/-}$ mice than in *Eprs*$^{+/+}$ mice. Finally, we collected brain tissue samples at 0–5 d after infection and assessed the histological features induced by VSV. Hematoxylin-and-eosin-stained brain sections from *Eprs*$^{+/-}$ mice showed greater infiltration by inflammatory cells (particularly around the lateral ventricle regions) than that of sections from *Eprs*$^{+/+}$ mice (**Fig. 3f**). In addition, immunohistochemical analysis of sectioned brains stained with antibody to G protein of VSV (anti-VSV) confirmed the presence of infected virus at sites around the inflammation, and viral clearance was slower in *Eprs*$^{+/-}$ mice than in *Eprs*$^{+/+}$ mice (**Fig. 3g**). Together these results supported the concept that EPRS was involved in mouse intracellular innate immune responses to viral infection.

## Infection-specific modification of EPRS

Published studies have shown that post-translational modifications, mainly phosphorylation, are key drivers of the release of ARSs from the MSC[9,23] and subsequent interaction with downstream effector molecules, as well as for activation of non-canonical functions[3,24]. For example, IFN-γ-dependent sequential phosphorylation of EPRS at

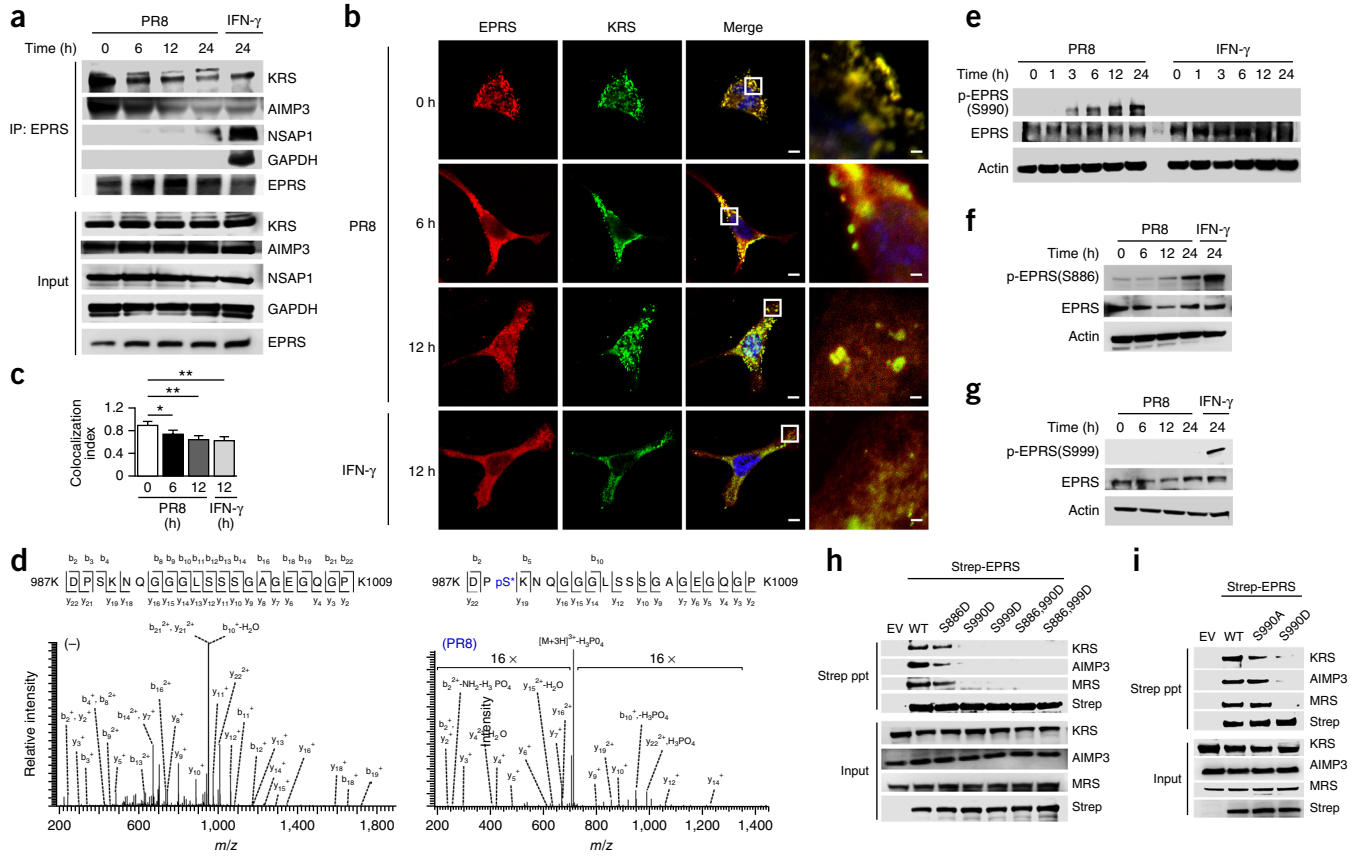


**Figure 4** Virus-induced phosphorylation of EPRS induces its release from the MSC. (**a**) Endogenous immunoprecipitation (IP), with anti-EPRS, followed by immunoblot analysis with anti-KRS and anti-AIMP3 (MSC components), and anti-NSAP1 and anti-GAPDH (GAIT complex components), at various times (above lanes) after infection of U937 cells by PR8-GFP (MOI = 3) or treatment with IFN-γ (500 units/ml). Input (bottom), immunoblot analysis in the cells above, without immunoprecipitation. (**b**) Confocal microscopy of the colocalization of endogenous EPRS (red) and KRS (green) in cells infected with PR8 (MOI = 5) or treated with IFN-γ (1,000 units/ml). Far right, enlargement of areas outlined at left. Scale bars, 10 μm (left and middle) or 1 μm (far right). (**c**) Colocalization index of EPRS and KRS in cells as in **b**. (**d**) Tandem mass spectrometry of a triply charged EPRS peptide (KDPSKNQGGGGLSSSGAGEGQGGPK in cells left uninfected (–; left) and of KDPpS*KNQGGGGLSSSGAGEGQGGPK (*, Ser990-phosphorylation site in cells infected with PR8 (right). (**e**–**g**) Immunoblot analysis of EPRS phosphorylated at Ser990 (**e**), Ser886 (**f**) or Ser999 (**g**) in U937 cells infected with PR8-GFP or treated with IFN-γ, for various times (above lanes). (**h**,**i**) Immunoblot analysis of 293T cells transfected (above lanes) with empty vector or vector encoding Strep-tagged wild-type EPRS (WT) or various combinations of three phosphomimetic forms of EPRS (S886D, S990D and S999D) (**h**) or the phosphorylation-resistant EPRS mutant S990A (**i**), assessed by Strep precipitation (ppt) and detection with anti-KRS, AIMP3 and anti-MRS. Input (bottom), immunoblot analysis without precipitation. $*P < 0.01$ and $**P < 0.001$ (Student's *t* test). Data are representative of three experiments with similar results, with three independent biological replicates (**a**,**b**,**e**–**i**) or three experiments (**c**; mean and s.d.).

Ser886 and Ser999 induces its release from the MSC to form the GAIT complex[13,25]. To assess the function of EPRS following viral infection, we infected U937 cells, which are the main cell type used for the study of EPRS in the context of IFN-γ activation[13], with PR8. Notably, the interaction of EPRS with KRS and AIMP3 was significantly reduced following virus infection (**Fig. 4a**), suggestive of dissociation of EPRS from the MSC. Immunoblot analysis with an antibody that targets NSAP1, a component of the pre-GAIT complex that directly binds EPRS via phosphorylation at Ser886 (ref. 13), revealed that EPRS bound weakly to NSAP1 at 12–24 h after infection. However, EPRS did not bind GAPDH (**Fig. 4a**), a constituent of GAIT complex that requires phosphorylation of EPRS at Ser999 to allow formation of a functional complex[13]. Virus-induced EPRS release from the MSC was further confirmed by co-immunoprecipitation of PR8-infected RAW264.7 macrophage lysates with anti-EPRS or anti-KRS (**Supplementary Fig. 4a**,**b**). Confocal microscopy analysis also revealed that EPRS colocalized with KRS, but the extent of colocalization was reduced following viral infection (**Fig. 4b**,**c** and **Supplementary Fig. 4c**). Notably, NSAP1, which is located mainly in the nucleus, slightly colocalized with EPRS at 12 h after infection (**Supplementary Fig. 4d**), consistent with the immunoblot analysis result (**Fig. 4a**), whereas the protein was translocated to the cytoplasm and showed marked IFN-γ-mediated colocalization with EPRS at 12 h after treatment (**Supplementary Fig. 4d**). These results suggested that a distinct virus-specific mechanism underlay EPRS activation.

To investigate the mechanism of EPRS activation and its role in antiviral responses, we next used a mass-spectrometry-based proteomics approach to identify specific post-translational modifications in streptavidin (Strep)-tagged EPRS ectopically expressed in HEK293T cells (**Supplementary Fig. 5a**). Phosphorylation of Ser886 was detected in both uninfected and infected cells, whereas Ser999 (which is phosphorylated following IFN-γ stimulation)[13] was unmodified under all conditions (**Supplementary Fig. 5b**–**d**). Unexpectedly, viral infection induced phosphorylation of EPRS at Ser990 (**Fig. 4d** and **Supplementary Fig. 5e**). To verify that finding, we generated a rabbit polyclonal antibody directed against this site by using the phosphorylated peptide $^{983}$DGQRKDP(p)SKNQGGG$^{996}$ (where '(p)S' indicates the phosphorylated residue Ser990) as an antigen

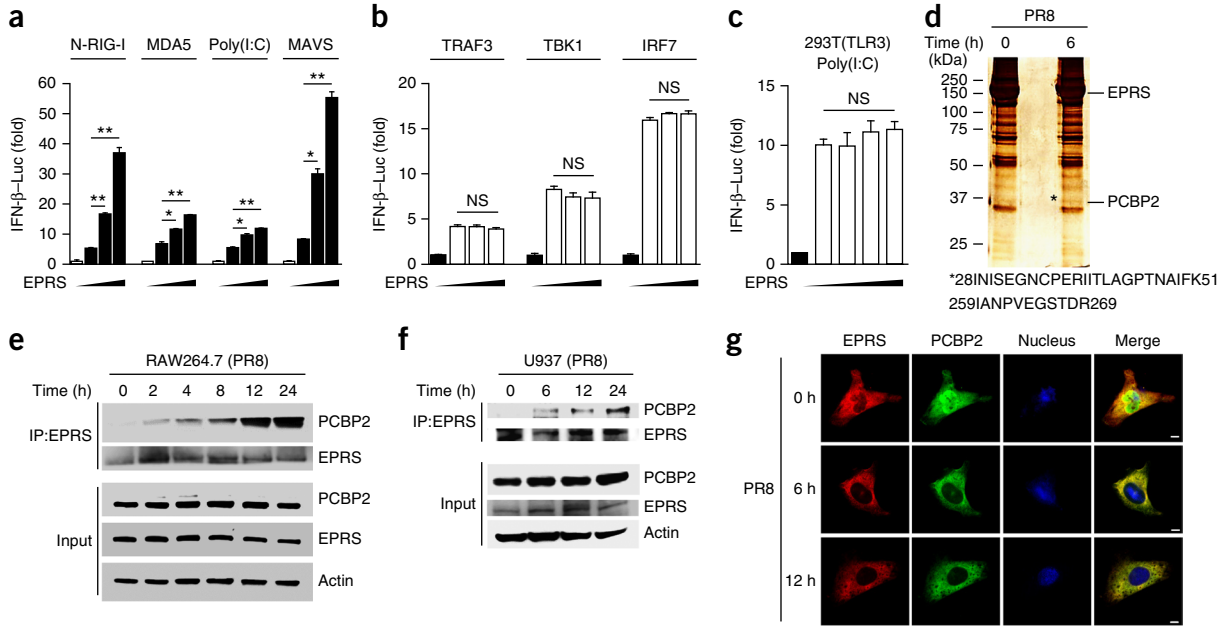


**Figure 5** EPRS interacts with PCBP2, a negative regulator of MAVS. (**a**,**b**) Luciferase assay (as in **Fig. 1b**) of *IFNB* promoter activation in 293T cells at 24 h after transfection (above plots) to express N-RIG-I, MDA5, poly(I:C) and MAVS (**a**) or TRAF3, TBK1 and IRF7 (**b**), and with increasing concentrations (0, 200 or 800 ng; wedges) of plasmid encoding FLAG-tagged EPRS (horizontal axes). (**c**) Luciferase assay (as in **Fig. 1b**) of *IFNB* promoter activation in Toll-like-receptor-3-expressing 293T cells (293T(TLR3)) transfected for 24 h with increasing concentrations (0, 50, 200 or 800 ng; wedges) of plasmid encoding FLAG-tagged EPRS (horizontal axis), followed by stimulation for 12 h with poly(I:C) (30 μg). (**d**) Silver staining (top) of Strep-EPRS complexes purified from 293T cells 24 h after transfection with a plasmid encoding Strep-EPRS, followed by infection for 6 h with PR8-GFP (MOI = 5): left margin, size in kilodaltons (kDa); right margin, Strep-tagged full-length EPRS (170 kDa); *, PCBP2 (38 kDa). Below, sequences of peptides identified by mass spectrometry. (**e**,**f**) Immunoassay of the interaction between EPRS and PCBP2 in PR8-infected RAW264.7 cells (**e**) and U937 cells (**f**), assessed by immunoprecipitation with anti-EPRS, followed by immunoblot analysis with anti-PCBP2 (input, as in **Fig. 4a**). (**g**) Confocal microcopy of endogenous EPRS (red) and PCBP2 (green) in HeLa cells at various times (left margin) after infection with PR8 (MOI = 5). Scale bars, 10 μm. NS, not significant ($P > 0.05$); $*P < 0.01$ and $**P < 0.001$ (Student's *t*-test). Data are representative of three experiments with similar results, with three independent biological replicates (**a**–**c**,**e**–**g**; mean and s.d. of triplicates in **a**–**c**) or one experiment (**d**).

(**Supplementary Fig. 5f**). Phosphorylation of EPRS at Ser990 gradually increased after infection of U937 cells with PR8 (**Fig. 4e**). In contrast, IFN-γ treatment did not induce phosphorylation of Ser990 (**Fig. 4e**). Similar results were obtained with other virus- or synthetic-RNA-treated cells (**Supplementary Fig. 5g–j**). We also detected small amounts of Ser886 phosphorylation in uninfected cells, which increased following PR8 infection, although the increase was less than that observed after stimulation by IFN-γ (**Fig. 4f**). Viral infection did not induce phosphorylation of Ser999, whereas IFN-γ stimulation clearly did (**Fig. 4g**). Furthermore, viral infection did not affect the secretion of IFN-γ or suppress the expression of ceruloplasmin, a target of the GAIT complex[4] (**Supplementary Fig. 5k–m**). Published studies using ectopically expressed phosphomimetics of EPRS have indirectly shown that phosphorylation of Ser886 and Ser999 induces the release of EPRS from the MSC[13]. Thus, we ectopically expressed wild-type EPRS and its phosphomimetic mutant (S990D) and a phosphorylation-resistant mutant (S990A) to assess their involvement in the MSC. S990D did not interact with the MSC components KRS, AIMP3or MRS (**Fig. 4h**,**i**), which (indirectly) indicated release of the modified EPRS from the MSC following infection. In contrast, association of the mutant S990A with MSC components was similar to that of wild-type EPRS (**Fig. 4i**), which confirmed that the dissociation of EPRS from the MSC was dependent on modification of EPRS at Ser990. Together these results suggested that virus-induced phosphorylation of EPRS at Ser990 induced its release from the MSC to execute a function distinct from its role in the IFN-γ-activated GAIT translational silencing pathway.

## EPRS interacts with PCBP2 to regulate MAVS signaling

Following the entry of a virus into cells, the intracellular sensor RIG-I is activated. RIG-I then interacts with MAVS to trigger a signaling cascade that culminates in the production of type I interferons[26]. Analysis of this signaling cascade revealed that EPRS increased RIG-I-, MDA5-, poly(I:C)- and MAVS-mediated activity of the *IFNB* promoter in a dose-dependent manner (**Fig. 5a**). However, we observed no substantial activation of the *IFNB* promoter in the presence of the signaling protein TRAF3, TBK1 or IRF7 (**Fig. 5b**) or in Toll-like-receptor-3-expressing HEK293T cells stimulated by poly(I:C) (**Fig. 5c**). These results suggested that EPRS is a positive regulator of the RIG-I- and MDA5-mediated type I interferon pathway and acts downstream of MAVS and upstream of the TRAF3 signaling axis.

To identify the EPRS-interacting molecules that regulate MAVS signaling during viral infection, we subjected Strep-EPRS–specific complexes from PR8-infected cells to proteomics analysis (**Fig. 5d**). We found MSC proteins but not GAIT proteins (NSAP1, GAPDH and L13a) (data not shown). Notably, EPRS interacted with PCBP2, a protein known to trigger ubiquitination and degradation of MAVS[22] after viral infection (**Fig. 5d–f**). Endogenous co-immunoprecipitation analysis confirmed the virus-induced interaction of EPRS with PCBP2 in RAW264.7 and U937 cells and that the interaction between the two proteins increased over time (**Fig. 5e**,**f**). Furthermore, and consistent with the findings of a published study[22,27], following viral infection, PCBP2 translocated from the nucleus to the cytoplasm, where it colocalized with EPRS (**Fig. 5g**).

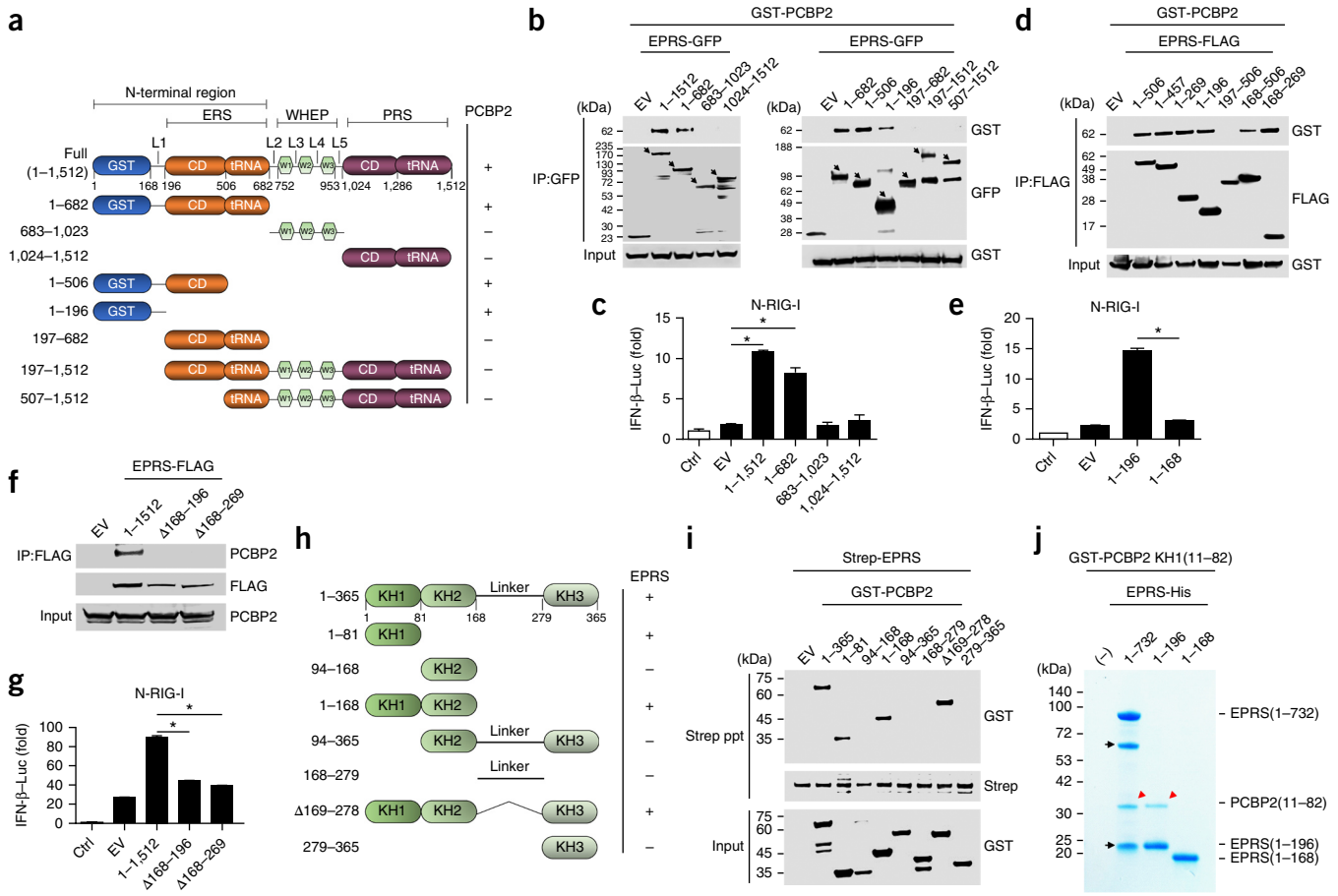


**Figure 6** Domain mapping required for the interaction between EPRS and PCBP2. (**a**) Full-length EPRS (top) and constructs of EPRS (below) containing various combinations of the GST-like domain (GST), catalytic domain (CD), tRNA-binding domain (tRNA), WHEP domains 1–3 (W1–W3) and linkers 1–5 (L1–L5), with (+) or without (–) binding to PCBP2 (right margin). (**b**,**d**,**f**) Immunoassay of 293T cells transfected with plasmid encoding GST-tagged PCBP2 and empty vector or plasmids encoding the GFP- or FLAG-tagged EPRS constructs in **a** (above lanes), assessed by co-immunoprecipitation (with anti-GFP or anti-FLAG) of the EPRS constructs with PCBP2, followed by immunoblot analysis with anti-GST or anti-GFP (**b**), anti-GST or anti-FLAG (**d**) or anti-PCBP2 or anti-FLAG (**f**) (input, as in **Fig. 4a**). (**c**,**e**,**g**) Luciferase assay (as in **Fig. 1b**) of *IFNB* promoter activation in 293T cells transfected with expression plasmids for N-RIG-I and the *IFNB* promoter, or without N-RIG-I (control (Ctrl)), together with empty vector or plasmids encoding the EPRS constructs in **a** (horizontal axes). (**h**) Full-length PCBP2 (top) and constructs containing or lacking (Δ) various combinations of PCBP2 domains (below), with (+) or without (–) binding to EPRS (right margin). (**i**) Immunoassay of the interaction of EPRS with PCBP2 in lysates of 293T cells expressing Strep-EPRS and various forms of GST-PCBP2, assessed by Strep precipitation followed by immunoblot analysis with anti-GST (input, as in **Fig. 4h,i**). (**j**) *In vitro* precipitation analyzing direct binding between various regions of EPRS (above lanes; amino acids 1–732, 1–196 and 1–168) and the PCBP2 KH1 domain (amino acids 11–82): black arrows, protein fragments derived from EPRS during purification (N-terminal sequences mapped to the MRFDD (amino acids 234–238) and MVTFI (amino acids 565–569) sequences of EPRS); red arrowheads, PCBP2 KH1 domain. $*P < 0.001$ (Student's *t*-test). Data are representative of three experiments with similar results, with three independent biological replicates (mean and s.d. of triplicates in **c**,**e**,**g**).

To identify the EPRS region responsible for the interaction with PCBP2, we generated plasmid constructs encoding various EPRS domains (**Fig. 6a**). We then performed co-immunoprecipitation to assess the interactions between each EPRS region and PCBP2. Our results revealed that the amino-terminal domain of EPRS (amino acids 1–196), which contains the glutathione *S*-transferase (GST)-like domain and linker region L1, was crucial for the interaction with PCBP2 and that it induced *IFNB* promoter activity comparable with that induced by full-length EPRS (**Fig. 6a–e**). However, the GST-like domain alone (amino acids 1–168) did not induce antiviral activity (**Fig. 6a–e**). These results suggested that the L1 region (amino acids 168–196) between the GST-like domain and ERS was necessary for both the interaction with PCBP2 and for the antiviral responses. We confirmed those results by showing that mutant EPRS with deletion of L1 did not interact with PCBP2 and showed diminished ability to activate the *IFNB* promoter (**Fig. 6f,g**).

On the other hand, we found that the amino-terminal K-homologous (KH1) domain (amino acids 1–81) of PCBP2, not the linker region, was sufficient for binding to EPRS (**Fig. 6h,i**). An *in vitro* binding assay revealed that PCBP2 KH1 specifically interacted with the GST and L1 regions of EPRS (amino acids 1–196) but not with the GST-like domain alone (amino acids 1–168) (**Fig. 6j** and **Supplementary Fig. 6a,b**), which further supported the finding that EPRS L1 was essential for interaction with PCBP2. Together these data indicated that Ser990-phosphorylation-driven release of EPRS from the MSC facilitated its interaction with PCBP2 and potentially regulated MAVS signaling.

We further assessed the non-translational function of EPRS in regulating antiviral immune responses through the use of a catalytic-null mutant generated by mutation of catalytic residues in the ERS domain[28] (**Supplementary Fig. 6c,d**) and PRS domain[29]. The *IFNB* promoter activity induced by non-translational mutants was comparable with that induced by wild-type EPRS (**Supplementary Fig. 6e**). Furthermore,

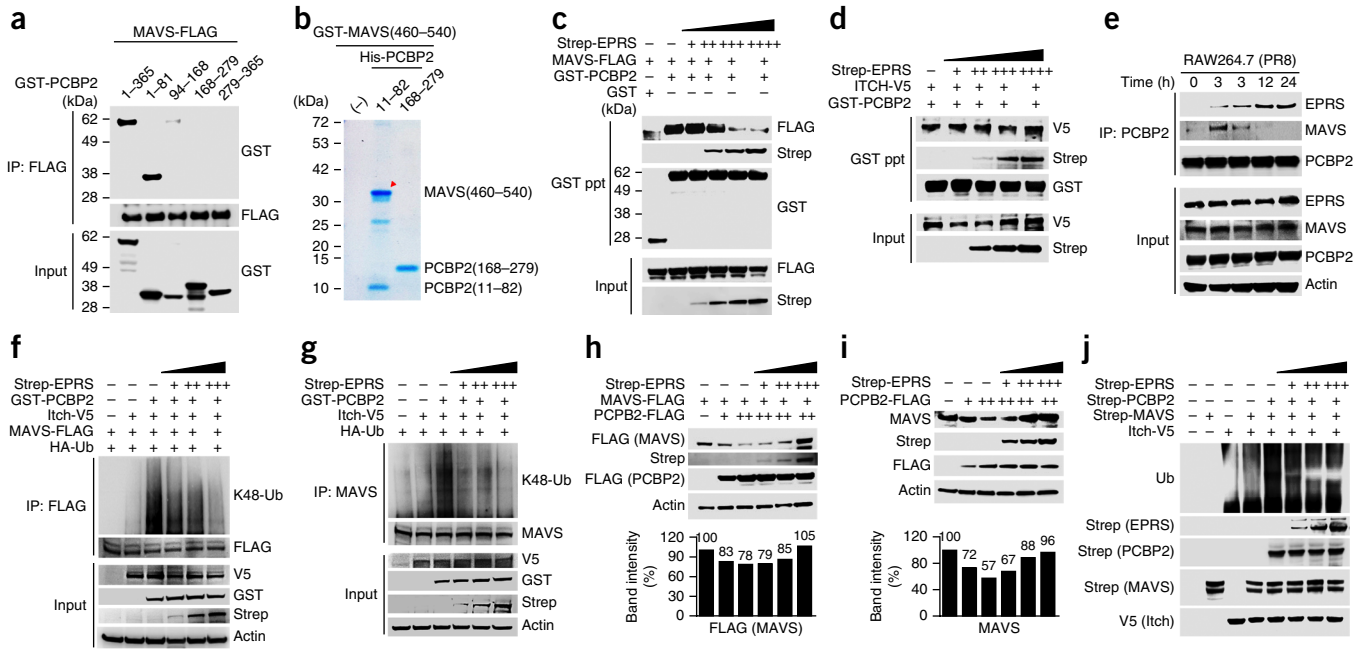


**Figure 7** EPRS blocks PCBP2-mediated ubiquitination and degradation of MAVS. (**a**) Immunoassay of the interaction of MAVS with PCBP2 in lysates of 293T cells transfected to express FLAG-tagged MAVS and plasmids encoding various GST-tagged constructs of PCBP2 (above lanes), assessed by co-immunoprecipitation with anti-FLAG and immunoblot analysis with anti-GST (input, as in **Fig. 4a** throughout). (**b**) *In vitro* precipitation assay (as in **Fig. 6j**) of cells as in **a**: arrowhead, MAVS. (**c**) GST-precipitation and immunoblot analysis of the interaction of PCBP2 with MAVS (top) or EPRS (bottom) in 293T cells transfected to express various combinations (above lanes) of FLAG-tagged MAVS and GST-tagged PCBP2 plus increasing amounts (wedges) of Strep-tagged EPRS, probed with anti-FLAG or anti-Strep. (**d**) GST-precipitation assay (as in **c**) of interactions between PCBP2 and Itch (top) and EPRS (bottom). (**e**) Immunoassay of the endogenous interactions between PCBP2 and EPRS or MAVS in lysates of PR8-infected RAW264.7 cells, assessed by immunoprecipitation with anti-PCBP2 (for endogenous PCBP2) and immunoblot analysis with anti-EPRS (top) or anti-MAVS (bottom). (**f**,**g**) Immunoblot analysis of exogenous MAVS (**f**) or endogenous MAVS (**g**) immunoprecipitated from lysates of 293T cells treated with the proteasome inhibitor MG-132 and then transfected to express various combinations (above lanes) of Strep-tagged EPRS, GST-tagged PCBP2, V5-tagged Itch, FLAG-tagged MAVS (**f** only) and hemagglutinin (HA)-tagged ubiquitin, probed with antibody to Lys48 (K48)-linked ubiquitin (K48-Ub) and other antibodies (right margin). (**h**,**i**) Immunoblot analysis (top) of exogenous MAVS (**h**) or endogenous MAVS (**i**) in 293T cells transfected to express FLAG-tagged PCBP2, FLAG-tagged MAVS (**h** only) and increasing amounts of Strep-tagged EPRS. Below, MAVS band intensity, normalized to that of actin (numbers above bars indicate specific intensity). (**j**) *In vitro* assay of the ubiquitination of purified Strep-tagged MAVS after incubation with ubiquitin, E1, E2, and a combination of purified Strep-tagged EPRS, Strep-tagged PCBP2 and V5-tagged Itch, assessed by immunoblot analysis with anti-ubiquitin. Data are representative of three experiments with similar results, with three independent biological replicates.



exogenous expression of wild-type EPRS or its enzymatically null mutant in 293T cells partially depleted of EPRS (**Supplementary Fig. 6f**) resulted in reduced replication of VSV-GFP and increased production of antiviral cytokines (**Supplementary Fig. 6g–k**). Thus, these results indicated that EPRS-mediated antiviral innate immunity was exclusively dependent on its non-catalytic region.

## EPRS protects MAVS from PCBP2-mediated ubiquitination

Published studies have shown that PCBP2 is expressed after viral infection and that it interacts with MAVS, which leads to ubiquitination of MAVS for proteasomal degradation[22,27]. Thus, we hypothesized that EPRS might protect MAVS by blocking PCBP2-mediated ubiquitination. When we re-evaluated the interaction of PCBP2 with MAVS, we found that MAVS specifically interacted with the KH1 domain of PCBP2, which is the same domain that bound EPRS (**Fig. 7a**,**b** and **Supplementary Fig. 7a**,**b**). Targeting of the same KH1 domain by EPRS and MAVS suggested that EPRS might compete with MAVS and thereby prevent its interaction with PCBP2 (**Figs. 6i** and **7a**). Indeed, the interaction between PCBP2 and MAVS was significantly reduced in the presence of EPRS (**Fig. 7c**). However, EPRS did not disrupt the binding of PCBP2 to the E3 ligase Itch (**Fig. 7d**). In addition, the interaction between PCBP2 and MAVS was not altered by the irrelevant protein leucyl-tRNA synthetase (**Supplementary Fig. 7c**,**d**), which suggested that EPRS specifically competed with MAVS to bind PCBP2 KH1. Those results were confirmed by endogenous interaction assays, which revealed that the binding of PCBP2 to MAVS gradually decreased, whereas its interaction with EPRS markedly increased, after infection of RAW264.7 cells with PR8 (**Fig. 7e**). These results suggested that EPRS acted to counter the endogenous binding of PCBP2 to MAVS in the infected cells.

PCBP2 accelerates ubiquitin-mediated degradation of MAVS by recruiting Itch[22]. Accordingly, we found that FLAG-tagged MAVS exogenously expressed in 293T cells was ubiquitinated by Itch and that the reaction markedly increased following the addition of PCBP2 (**Fig. 7f**). EPRS-deficient cells were more susceptible to ubiquitination of MAVS (**Supplementary Fig. 7e**). However, the addition of EPRS inhibited PCBP2-mediated ubiquitination of MAVS in a dose-dependent manner (**Fig. 7f**). Likewise, endogenous ubiquitination of MAVS was greatly enhanced by PCBP2 but was significantly attenuated in the presence of EPRS (**Fig. 7g**). Consistent with the results of the ubiquitination assay, both exogenous MAVS (**Fig. 7h**) and endogenous MAVS (**Fig. 7i**) were degraded by PCBP2, but were rescued from this degradation by the addition of EPRS. Finally, analysis of a cell-free system reconstituted with purified EPRS revealed much less PCBP2-mediated ubiquitination of MAVS (**Fig. 7j**). In addition, we assessed the non-translational function of EPRS in

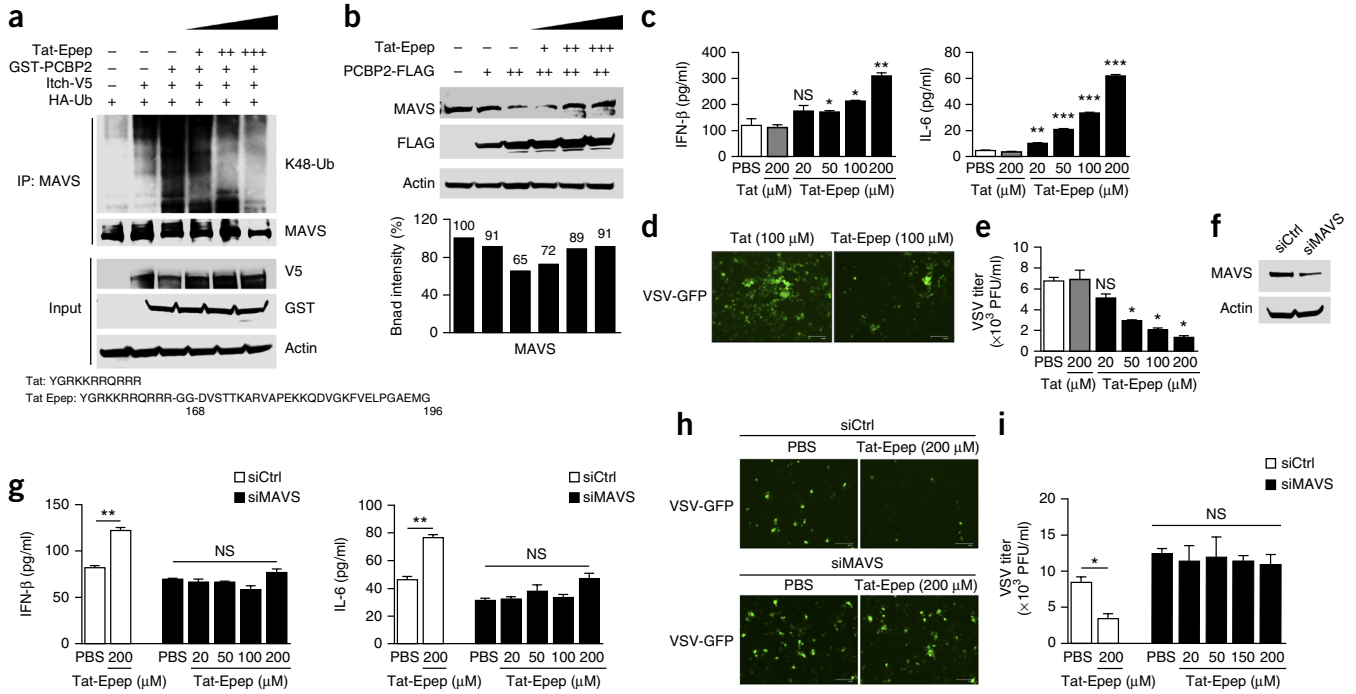


**Figure 8** An EPRS-derived L1 peptide has antiviral activity. (**a**) Immunoassay (top) of 293T cells transfected with various combinations (above lanes) plasmids encoding GST-tagged PCBP2, V5-tagged Itch and hemagglutinin-tagged ubiquitin and increasing amounts (wedges) of Tat-Epep (20, 50 and 100 μM), assessed by immunoprecipitation with anti-MAVS (to precipitate endogenous MAVS), followed by immunoblot analysis with antibody to K48 ubiquitin (input, as in **Fig. 4a**). Below, sequence of Tat and Tat-Epep. (**b**) Immunoblot analysis (top) of endogenous MAVS in 293T cells transfected to express FLAG-tagged PCBP2 and increasing amounts of Tat-Epep (as in **a**). Below, MAVS band intensity (presented as in **Fig. 7h**,**i**). (**c**) Secretion of IFN-β and IL-6 by VSV-infected RAW264.7 cells treated with PBS (negative control) or various concentrations (horizontal axis) of Tat or Tat-Epep. (**d**) Fluorescence microscopy of RAW264.7 cells infected with VSV-GFP and treated with Tat or Tat-Epep (above images). (**e**) Viral titers in infected RAW264.7 cells as in **c**. (**f**) Immunoblot analysis of MAVS in RAW264.7 cells transfected with non-targeting control siRNA (siCtrl) or MAVS-specific siRNA (siMAVS) and treated as in **c**. (**g**–**i**) Secretion of IFN-β and IL-6 (**g**) and microscopy (**h**) viral titers (**i**) of MAVS-deficient RAW264.7 cells transfected with siRNA as in **f** and infected and treated as in **c**. Scale bars (**d**,**h**), 125 μm. $*P < 0.05$, $**P < 0.01$ and $***P < 0.001$ (Student's *t*-test). Data are representative of three experiments with similar results, with least three independent biological replicates (mean and s.d. of triplicates in **c**,**e**,**g**,**i**).

regulating MAVS and found that non-catalytic EPRS protected MAVS from PCBP2-mediated ubiquitination in a manner similar to that used by wild-type EPRS (**Supplementary Fig. 7f**,**g**). Thus, these results showed that EPRS specifically blocked PCBP2-mediated negative regulation of MAVS and thereby maintained strong antiviral immune responses.

We next assessed the correlation between EPRS phosphorylation and its antiviral effects in HEK293 cells partially depleted of EPRS, which were much more susceptible to ubiquitination of MAVS (**Supplementary Fig. 7h**); we reconstituted the cells with wild-type EPRS, the phosphorylation-resistant mutant S990A or the phosphomimetic mutant S990D. We first assessed their effects on the ubiquitination of MAVS and found that the S990A mutant was unable to restore virus-induced ubiquitination of MAVS, whereas wild-type EPRS and S990D considerably inhibited the ubiquitination of MAVS (**Supplementary Fig. 7i**). Accordingly, the amount of IFN-β and IL-6 produced in response to viral infection was greater for cells reconstituted with wild-type EPRS or S990D than for cells reconstituted with S990A (**Supplementary Fig. 7j**,**k**). Consequently, wild-type EPRS and S990D markedly inhibited viral replication, whereas S990A was unable to rescue virus-infected cells (**Supplementary Fig. 7l**–**n**). Together these results showed that virus-infection-induced phosphorylation of EPRS at Ser990 was the driving force that led to the antiviral roles of EPRS in regulating MAVS we identified here.

## An EPRS-derived peptide shows antiviral activity

Thus far, we had found that the EPRS L1 region (amino acids 168–196) was both essential for interaction with PCBP2 and responsible for promoting antiviral type I interferon signaling. We next designed a cell-penetrating peptide by fusing the protein-transduction domain of the human immunodeficiency virus type 1 regulatory protein Tat[30] to the EPRS L1 region (called 'Tat-Epep' here) and assessed its effects on antiviral activity. Tat-Epep compromised PCBP2-mediated endogenous ubiquitination of MAVS (**Fig. 8a**) and restored the cellular expression of MAVS (**Fig. 8b**). Tat-Epep also increased the production of IFN-β and IL-6 in virus-infected cells (**Fig. 8c**) and reduced VSV replication in RAW264.7 cells in a dose-dependent manner (**Fig. 8d**,**e**). However, Tat-Epep showed no substantial antiviral activity in RAW264.7 cells infected with HSV (**Supplementary Fig. 8a**–**c**), which suggested that Tat-Epep was specific to infection with RNA viruses. To confirm the MAVS specificity of Tat-Epep, we knocked down MAVS in RAW264.7 cells, infected the cells with VSV-GFP and then treated them with Tat-Epep. Tat-Epep did not reduce viral replication or affect cytokine induction in MAVS-deficient cells (**Fig. 8f**–**i**). Tat-Epep had no effect on the viability of RAW264.7 or 293T cells at the concentrations tested (**Supplementary Fig. 8d**,**e**), which indicated that the diminished viral titer was not a result of peptide-mediated cytotoxicity. These data suggested that Tat-Epep might be a potential anti-RNA virus agent that promotes MAVS stability and production of type I interferons.

## DISCUSSION

The cytoplasmic MSC might serve as a reservoir of ARSs that can respond rapidly to cellular stresses without calling for *de novo* transcription and translation[2]. We identified an antiviral function for EPRS, an MSC constituent, both *in vitro* and *in vivo*. Instead of IFN-γ-induced phosphorylation of EPRS at Ser999, which is critical for activation of the GAIT system, we identified a previously unknown phosphorylation site (Ser990) that was phosphorylated following viral infection. It is noteworthy that Ser990 and Ser999, which are only nine residues apart, are located in the unstructured linker region (approximately amino acids 947–1020), which is between the third WHEP domain[31] and the PRS domain[32], and dictate different functions of EPRS. The use of multiple and selective phosphorylation sites in a high accessibility region might represent a highly efficient method of switching EPRS function in response to different stimuli. In this way, EPRS exhibits a phosphorylation 'code' similar to that of other key signaling proteins that act as nexuses for multiple pathways, as exemplified by retinoblastoma protein[33,34].

Bifunctional EPRS exists in dimeric form (mediated by antiparallel dimerization of the carboxy-terminal PRS domain)[32] and resides at the exterior of the MSC[4,9,11,12]. Size-exclusion chromatography revealed that the amino-terminal GST and ERS domains were not involved in the dimerization (data not shown). This unique dimeric conformation of EPRS might be important for maintaining the integrity of the MSC, as both amino-terminal GST-like domains interact with the respective GST-like domains in the dimeric AIMP2 molecule (core scaffold protein of MSC)[11]. The central WHEP domains located between the ERS and PRS domains might have a role in associating the catalytic domains with the MSC. Accordingly, phosphorylation of the serine residues in the linker region between the third WHEP domain and PRS might cause conformational changes and thereby weaken the binding of EPRS to the MSC and facilitate its release. Such unique and efficient properties of EPRS might be critical for maintaining immunological homeostasis via immunostimulatory activity following viral infection and contrasting anti-inflammatory activity after stimulation with IFN-γ. The precise mechanism by which phosphorylation induces the release of EPRS from the MSC via conformational changes should be explored further by kinase-profiling and structural-analysis studies.

MAVS acts as a critical adaptor in the RLR signaling pathway to control viral replication[35]. Cells employ many diverse mechanisms to tightly regulate MAVS and prevent unwanted responses following viral infection[36]. In addition to PCBP2 and Itch, several E3 ligases (Smurf1 (ref. 37), Gp78 (ref. 38) and TRIM25 (ref. 39)) regulate levels of MAVS after viral infection. Although we did not investigate the affinities of the MAVS-PCBP2 and EPRS-PCBP2 interactions, the kinetics for each were different in virus-infected cells. As has been reported for Sendai virus[22], we observed a virus-induced interaction between PCBP2 and MAVS at 3 h after PR8 infection. Nonetheless, we found that EPRS constitutively prevented the association between PCBP2 and MAVS after viral infection, which correlated with the kinetics of Ser990 phosphorylation. In addition, it is clear that EPRS positively regulates the antiviral immune response in mice. On the other hand, IFN-γ produced by natural killer cells and T cells during the late stages of an immune response activates the GAIT system and prevents chronic and excessive accumulation of inflammatory proteins[4]. Following viral infection, the antiviral role of EPRS seems to dominate over GAIT-mediated gene silencing by increasing the production of type I interferons to maintain host fitness. Future studies will help to delineate the dual roles that EPRS might have in regulating immune responses. Such dual functions could include enhancing antiviral immune responses and GAIT complex formation (thereby avoiding damage to the cell as a result of excessive inflammation); these functions might depend on several parameters, including temporal kinetics, different types of stress or stimuli, and the amount of pathogen. In conclusion, this newly identified function of EPRS (positive regulation of MAVS during RLR signaling) has revealed the functional importance of the MSC as a regulator of immune responses to viral infection.

## METHODS

Methods and any associated references are available in the online version of the paper.

**Accession codes.** GEO: microarray data, GSE75699.

*Note: Any Supplementary Information and Source Data files are available in the online version of the paper.*

### ACKNOWLEDGMENTS

Supported by the KRIBB Initiative Program (KGM4541622 to M.H.K.), the National Research Foundation of Korea, funded by the Ministry of Science, ICT & Future Planning of Korea (NRF-2010-0029767 and 2014R1A2A1A01005971 to M.H.K.; NRF-M3A6A4-2010-0029785 to S.K.; and 2015020957 to J.-S.L.), the Korea Institute of Oriental Medicine (K12050 to J.-S.L.), the Ministry for Food, Agriculture, Forestry and Fisheries (315044031SB010 to J.-S.L.) and the Korea Health Industry Development Institute (HI14C3484 to C.L.).

### AUTHOR CONTRIBUTIONS

E.-Y.L. and H.-C.L. performed most of the experiments with help from H.-K.K., S.Y.J., J.H., J.-H.K. and T.-H.K. S.-J.P. and C.L. performed mass spectrometry. Y.-H.K. and C.-H.L. performed immunohistochemical analysis. J.H.K., S.-Y.K. and Y.-K.C. performed RNA-seq analysis. A.A., J.U.J., P.L.F. and S.K. contributed to the discussion and provided critical reagents. E.-Y.L., J.-S.L. and M.H.K. designed the study and wrote the manuscript. All of the authors helped with data analysis.

### COMPETING FINANCIAL INTERESTS

The authors declare no competing financial interests.



1. Guo, M., Yang, X.L. & Schimmel, P. New functions of aminoacyl-tRNA synthetases beyond translation. *Nat. Rev. Mol. Cell Biol.* **11**, 668–674 (2010).
2. Ray, P.S., Arif, A. & Fox, P.L. Macromolecular complexes as depots for releasable regulatory proteins. *Trends Biochem. Sci.* **32**, 158–164 (2007).
3. Sampath, P. *et al.* Noncanonical function of glutamyl-prolyl-tRNA synthetase: gene-specific silencing of translation. *Cell* **119**, 195–208 (2004).
4. Mukhopadhyay, R., Jia, J., Arif, A., Ray, P.S. & Fox, P.L. The GAIT system: a gatekeeper of inflammatory gene expression. *Trends Biochem. Sci.* **34**, 324–331 (2009).
5. Guo, M. & Schimmel, P. Essential nontranslational functions of tRNA synthetases. *Nat. Chem. Biol.* **9**, 145–153 (2013).
6. Tandle, A.T. *et al.* Endothelial monocyte activating polypeptide-II modulates endothelial cell responses by degrading hypoxia-inducible factor-1alpha through interaction with PSMA7, a component of the proteasome. *Exp. Cell Res.* **315**, 1850–1859 (2009).
7. Kim, S., You, S. & Hwang, D. Aminoacyl-tRNA synthetases and tumorigenesis: more than housekeeping. *Nat. Rev. Cancer* **11**, 708–718 (2011).
8. Kwon, N.H. *et al.* Dual role of methionyl-tRNA synthetase in the regulation of translation and tumor suppressor activity of aminoacyl-tRNA synthetase-interacting multifunctional protein-3. *Proc. Natl. Acad. Sci. USA* **108**, 19635–19640 (2011).
9. Ofir-Birin, Y. *et al.* Structural switch of lysyl-tRNA synthetase between translation and transcription. *Mol. Cell* **49**, 30–42 (2013).
10. Kim, D.G. *et al.* Interaction of two translational components, lysyl-tRNA synthetase and p40/37LRP, in plasma membrane promotes laminin-dependent cell migration. *FASEB J.* **26**, 4142–4159 (2012).
11. Cho, H.Y. *et al.* Assembly of multi-tRNA synthetase complex via heterotetrameric glutathione transferase-homology domains. *J. Biol. Chem.* **290**, 29313–29328 (2015).
12. Wolfe, C.L., Warrington, J.A., Treadwell, L. & Norcum, M.T. A three-dimensional working model of the multienzyme complex of aminoacyl-tRNA synthetases based on electron microscopic placements of tRNA and proteins. *J. Biol. Chem.* **280**, 38870–38878 (2005).
13. Arif, A. *et al.* Two-site phosphorylation of EPRS coordinates multimodal regulation of noncanonical translational control activity. *Mol. Cell* **35**, 164–180 (2009).

14. Jia, J., Arif, A., Ray, P.S. & Fox, P.L. WHEP domains direct noncanonical function of glutamyl-prolyl tRNA synthetase in translational control of gene expression. *Mol. Cell* **29**, 679–690 (2008).
15. Vyas, K. *et al.* Genome-wide polysome profiling reveals an inflammation-responsive posttranscriptional operon in γ interferon-activated monocytes. *Mol. Cell. Biol.* **29**, 458–470 (2009).
16. Schoenborn, J.R. & Wilson, C.B. Regulation of interferon-γ during innate and adaptive immune responses. *Adv. Immunol.* **96**, 41–101 (2007).
17. Schroder, K., Hertzog, P.J., Ravasi, T. & Hume, D.A. Interferon-γ: an overview of signals, mechanisms and functions. *J. Leukoc. Biol.* **75**, 163–189 (2004).
18. Akira, S., Uematsu, S. & Takeuchi, O. Pathogen recognition and innate immunity. *Cell* **124**, 783–801 (2006).
19. McWhirter, S.M., Tenoever, B.R. & Maniatis, T. Connecting mitochondria and innate immunity. *Cell* **122**, 645–647 (2005).
20. Gack, M.U. *et al.* TRIM25 RING-finger E3 ubiquitin ligase is essential for RIG-I-mediated antiviral activity. *Nature* **446**, 916–920 (2007).
21. Belgnaoui, S.M. *et al.* Linear ubiquitination of NEMO negatively regulates the interferon antiviral response through disruption of the MAVS-TRAF3 complex. *Cell Host Microbe* **12**, 211–222 (2012).
22. You, F. *et al.* PCBP2 mediates degradation of the adaptor MAVS via the HECT ubiquitin ligase AIP4. *Nat. Immunol.* **10**, 1300–1308 (2009).
23. Yang, X.L. Structural disorder in expanding the functionome of aminoacyl-tRNA synthetases. *Chem. Biol.* **20**, 1093–1099 (2013).
24. Sajish, M. *et al.* Trp-tRNA synthetase bridges DNA-PKcs to PARP-1 to link IFN-γ and p53 signaling. *Nat. Chem. Biol.* **8**, 547–554 (2012).
25. Arif, A., Jia, J., Moodt, R.A., DiCorleto, P.E. & Fox, P.L. Phosphorylation of glutamyl-prolyl tRNA synthetase by cyclin-dependent kinase 5 dictates transcript-selective translational control. *Proc. Natl. Acad. Sci. USA* **108**, 1415–1420 (2011).
26. Papatriantafyllou, M. Innate immunity: MAVS build-ups for defence. *Nat. Rev. Immunol.* **11**, 570–571 (2011).
27. Xia, P. *et al.* IRTKS negatively regulates antiviral immunity through PCBP2 sumoylation-mediated MAVS degradation. *Nat. Commun.* **6**, 8132 (2015).
28. Sekine, S. *et al.* ATP binding by glutamyl-tRNA synthetase is switched to the productive mode by tRNA binding. *EMBO J.* **22**, 676–688 (2003).
29. Son, J. *et al.* Conformational changes in human prolyl-tRNA synthetase upon binding of the substrates proline and ATP and the inhibitor halofuginone. *Acta Crystallogr. D Biol. Crystallogr.* **69**, 2136–2145 (2013).
30. van den Berg, A. & Dowdy, S.F. Protein transduction domain delivery of therapeutic macromolecules. *Curr. Opin. Biotechnol.* **22**, 888–893 (2011).
31. Cahuzac, B., Berthonneau, E., Birlirakis, N., Guittet, E. & Mirande, M. A recurrent RNA-binding domain is appended to eukaryotic aminoacyl-tRNA synthetases. *EMBO J.* **19**, 445–452 (2000).
32. Zhou, H., Sun, L., Yang, X.L. & Schimmel, P. ATP-directed capture of bioactive herbal-based medicine on human tRNA synthetase. *Nature* **494**, 121–124 (2013).
33. Rubin, S.M. Deciphering the retinoblastoma protein phosphorylation code. *Trends Biochem. Sci.* **38**, 12–19 (2013).
34. Burkhart, D.L. & Sage, J. Cellular mechanisms of tumour suppression by the retinoblastoma gene. *Nat. Rev. Cancer* **8**, 671–682 (2008).
35. Yoneyama, M. *et al.* The RNA helicase RIG-I has an essential function in double-stranded RNA-induced innate antiviral responses. *Nat. Immunol.* **5**, 730–737 (2004).
36. Takeuchi, O. & Akira, S. Pattern recognition receptors and inflammation. *Cell* **140**, 805–820 (2010).
37. Wang, Y., Tong, X. & Ye, X. Ndfip1 negatively regulates RIG-I-dependent immune signaling by enhancing E3 ligase Smurf1-mediated MAVS degradation. *J. Immunol.* **189**, 5304–5313 (2012).
38. Jacobs, J.L., Zhu, J., Sarkar, S.N. & Coyne, C.B. Regulation of mitochondrial antiviral signaling (MAVS) expression and signaling by the mitochondria-associated endoplasmic reticulum membrane (MAM) protein Gp78. *J. Biol. Chem.* **289**, 1604–1616 (2014).
39. Castanier, C. *et al.* MAVS ubiquitination by the E3 ligase TRIM25 and degradation by the proteasome is involved in type I interferon production after activation of the antiviral RIG-I-like receptors. *BMC Biol.* **10**, 44 (2012).

## ONLINE METHODS

**Cell culture and transfection.** HEK293T, HeLa, MDCK, Vero, RAW264.7, MEF, RIG-I-sufficient and RIG-I-deficient MEF[20] cells were maintained in Dulbecco's Modified Eagle's medium (DMEM, Gibco-BRL) supplemented with 10% FBS (FBS, Gibco-BRL) and 1% penicillin-streptomycin (Gibco-BRL). U937 cells were grown in RPMI 1640 media (Gibco-BRL) containing 10% FBS and 1% penicillin-streptomycin. HEK293T, HeLa, MDCK, Vero, RAW264.7, and U937 cells were obtained from the American Type Culture Collection. HEK293T cells expressing human Toll-like receptor 3 were purchased from InvivoGen (293-htlr3). BMDMs were isolated from 5- to 6-week-old mice, and red blood cells were lysed with ammonium-chloride-potassium (ACK) lysing buffer (Gibco-BRL). BMDMs were then cultured in DMEM containing 10% FBS, 10% L929 cell-conditioned medium, and GM-CSF (R&D Systems). The medium was replaced with fresh complete medium every 2 d. Cells were used for the experiments on day 7. Stable RAW264.7 cells in which EPRS was knocked down were established by treatment with short hairpin RNA after selection with 2 μg/ml of puromycin for at least 2 weeks. RAW264.7 cells stably expressing pIRES or pIRES-EPRS-FLAG were established by transfection with the corresponding DNA constructs and maintained in DMEM supplemented with puromycin (1 μg/ml). HEK293T cells were transfected with DNA plasmid constructs using the X-tremeGENE HP DNA transfection reagent (Roche). U937, RAW264.7 and BMDM cells were transfected with nucleotransfector (Lonza) and immediately transferred to Opti-MEM medium (Gibco-BRL) for 6 h, followed by culture in complete medium containing 10% FBS for 24 h.

**Generation of partially EPRS-depleted cells.** To establish the EPRS-depleted HEK293T cell line, an EPRS-targeted RNA-guided endonuclease (RGEN) system was generated using CRISPR/Cas9 (ToolGen). The target EPRS sequence in the RGEN plasmid is listed in **Supplementary Table 1**. To enrich EPRS-depleted cells, they were transfected with the surrogate reporter plasmid pRG2S, which contains red-fluorescent protein and a puromycin selection marker. At 48 h after transfection, the cells were serially diluted to obtain a single cell-derived colony and grown for 2 weeks in DMEM containing 10% FBS, 1% penicillin-streptomycin, and 2 μg/ml puromycin. More than 30 single cell colonies were collected, and the expression of EPRS was examined by immunoblotting. Because EPRS is essential for cell viability, the cell colony showing the lowest EPRS expression was selected to evaluate EPRS function in regulating antiviral immunity. For convenience, the cell line partially depleted of EPRS is referred to as 'sgEPRS'.

**Mice and viral infection.** C57BL/6 EPRS$^{tm1b}$ heterozygous knockout mice[40] were obtained from the Toronto Center for Phenogenomics and maintained in a specific pathogen-free facility on a 12-h light/dark cycle at 22 ± 2 °C with free access to food and water. Offspring were genotyped by PCR using the following primers: A: 5′-CTACTGTGCTGAATGAAAAGTGCC-3′ and B: 5′- GGTAGAAGTGCTAAGTAGGATGAGG-3′ (specific for the 218 bp WT band); and C: 5′-CCATTACCAGTTGGTCTGGTGTC-3′ and D: 5′-TGCCTGTGACCACCAATAAGAAAGCC-3′ (specific for the 462 bp mutant band). All mice were euthanized by $CO_2$ asphyxiation. All animal experiments were approved by the Institutional Animal Use and Care Committee of the Korea Research Institute of Bioscience and Biotechnology and the Institutional Animal Care and Use Committee of Bioleaders Corporation (Reference number BLS-ABSL-14-014), and were performed in accordance with the Guide for the Care and Use of Laboratory Animals (published by the US National Institutes of Health). For the viral infection experiments, age- and sex-matched mice were infected with VSV-Indiana ($2 \times 10^8$ PFU per mouse) or VSV-GFP ($2 \times 10^8$ pfu per mouse) via intravenous injection into the tail vein. All *in vivo* experiments were performed by blind tests. No randomization was used in this study and no mice were excluded from analysis.

**Reagents and antibodies.** The antibodies used for the immunoblotting and immunofluorescence experiments are listed in **Supplementary Table 2**. Other reagents and materials included MG-132 (Sigma), puromycin (Gibco-BRL), poly(I:C) (InvivoGen), IFN-γ (R&D Systems), digitonin (Sigma), protein A/G PLUS-agarose (sc-2003, Santa Cruz Biotechnology), Glutathione Sepharose 4 Fast Flow (17-5132-01, GE Healthcare), anti-FLAG M2 affinity gel (A2220, Sigma), Strep-Tactin Sepharose (2-1201-002, IBA), Ni-NTA agarose (30230, Qiagen), GFP-trap (gta-20, ChromoTek), and a Superdex 200 10/300 GL column (GE Healthcare).

**Plasmid construction.** Several EPRS (GenBank accession number NM_004446.2) constructs bearing FLAG, Strep, His and GFP tags were generated. Briefly, a series of PCR-amplified truncated EPRS mutants harboring each domain were subcloned into GFP-, Strep-, His- or FLAG-tag-containing vectors. Phosphomimetic mutants of EPRS (S886D, S990D, S999D, S886D,S990D, and S886D,S999D) and a phosphorylation-resistant mutant, S990A, were generated. To generate a catalytically inactive ERS domain in EPRS, the catalytic residues were mutated (ATP-binding residues R201L and R395L and glutamate-binding residues S434A and K435L) based on the structure of *Thermus thermophiles* ERS[28]. Mutation of R1152L was performed to generate a catalytically inactive PRS[29] domain within EPRS. All mutations were introduced by PCR using a QuikChange site-directed mutagenesis kit (Stratagene). The PCR primers used for site-directed mutagenesis are listed in **Supplementary Table 1**. Specific FLAG-, Strep-, His- and GST-tagged full-length and several truncated PCBP2 mutants were also generated. MAVS was cloned into FLAG-, GST- or Strep-tag containing vectors, and MSC genes [KRS, glutaminyl-tRNA synthetase (QRS), AIMP1, AIMP2, AIMP3, leucyl-tRNA synthetase and MRS] were cloned into a Strep-tagged vector.

**RNA-seq analysis.** Primary normal human bronchial epithelial (NHBE) cells were purchased from ScienCell Research Laboratories and differentiated as previously described[41]. Monolayers of NHBE cells were infected with A/PR/8/34 influenza virus (MOI = 1) for 8 or 24 h. Total RNA was isolated from the infected cells using the RNeasy RNA extraction Mini-Kit (Qiagen) and the quality of the RNA was confirmed by agarose gel electrophoresis. The sequencing library was prepared using the TruSeq RNA sample preparation kit v2 (Illumina), as previously reported[42]. In brief, mRNA derived from total RNA using poly-T oligo-attached magnetic beads was fragmented and converted into cDNA. Adapters were ligated to the cDNA and the fragments were amplified by PCR. Paired-end sequencing (101 × 2) was performed using a Hiseq-2000 (Illumina). Each condition was sequenced in duplicate. Reference genome sequence data from *Homo sapiens* were obtained from the University of California Santa Cruz Genome Browser Gateway (assembly ID: hg19). The reference genome index was built using SAMtools (v. 0.1.19) and the Bowtie2-build component of Bowtie2 (v. 2.1.0). Reads were mapped to the reference genome using Tophat2 (v. 2.0). The number of reads per kilobase per million mapped reads (rpkm) for each gene of 46,895 RefSeq (UCSC hg19) gene models was calculated using Cufflinks (v. 2.2.1). Heat maps were constructed using Mev (v. 4.9.0). Statistical analyses and graph construction were performed using R (v. 3.1.0) and PYTHON (v. 2.7.6). The RNA-Seq data discussed in this study have been deposited in NCBI's Gene Expression Omnibus (GEO) under accession code GSE75699.

**Luciferase assay.** HEK293T cells were transfected with a mixture containing a luciferase reporter plasmid, a renilla luciferase internal control vector (phRL-TK; Promega), and each of the indicated plasmids. The reporter gene assay was performed at 24 h after transfection using a luminometer (Promega) and the dual-luciferase reporter assay system (Promega). Data are expressed in terms of relative firefly luciferase activity normalized against renilla luciferase activity. Promoter activity in cells expressing only reporter and renilla plasmids was measured as a control.

**RNA interference.** Cells were transfected with duplex siRNA using the *Trans* IT-TKO transfection reagent (Mirus), according to the manufacturer's protocol. The sequence of the EPRS-specific siRNA is provided in **Supplementary Table 1**. A non-targeting siRNA was used as a control. Cells were incubated with the siRNA or control for 36–48 h before exposure to viruses.

**Virus replication assay.** Cells were infected with virus in reduced serum (1% FBS)-containing media for 2 h. Excess virus was removed by replacing the culture supernatant with complete medium. Viral titers were determined in MDCK cells (PR8-GFP) or Vero cells (VSV-GFP or HSV-GFP) using a standard plaque assay. Homogenates of freeze-thawed tissue extracts were used for plaque counting when titrating viruses present in mouse tissues.

The replication of GFP-tagged virus was measured using the fluorescence module of the GloMax Multi-Microplate Multimode Reader (Promega). Images were acquired using a Nikon eclipse Ti microscope fitted with a 20 × 1.4 NA Plan-Apochromat objective lens.

**ELISA.** Cytokine concentrations were measured by ELISA of infected cell culture supernatants or mouse serum. The following ELISA kits were used according to the manufacturer's instructions: mouse or human IL-6 (BD Biosciences), IFN-α and IFN-β (PBL interferon source), and IFN-γ (KOMA).

**Quantitative real-time PCR.** Total RNA was extracted from cells and murine tissues using the RNeasy RNA extraction Mini-Kit (Qiagen). cDNA was synthesized using the Enzynomix kit (Enzynomix) and quantitative PCR was performed using gene-specific primer sets (Bioneer) and SYBR Green PCR Master Mix (Roche). Real-time PCR was performed using a Rotor-Gene Q instrument (Qiagen), according to the manufacturer's instructions. Data were normalized against *Gapdh* expression. Relative expression was calculated using the delta-delta CT method. The sequences of the primers used are listed in **Supplementary Table 1**.

**Immunoblot analysis and immunoprecipitation.** For immunoblot analysis, cells were lysed with RIPA buffer (20 mM Tris-HCl, pH 7.4, 150 mM NaCl, 1% NP-40, and 1 mM EDTA) containing a protease inhibitor cocktail and a phosphatase inhibitor cocktail (Roche). Whole cell lysates (50–100 μg) were subjected to SDS-PAGE followed by immunoblotting with the indicated antibodies. To detect phosphorylated proteins, cell lysates were prepared in Phosphosafe extraction buffer (Millipore) containing protease inhibitor cocktail at 4 °C. For immunoprecipitation, cell lysates were pre-cleared by incubation with protein A beads for 1 h at 4 °C. The pre-cleared cell lysates were incubated overnight at 4 °C with the indicated antibodies, followed by incubation with 30 μl of protein A/G PLUS-agarose beads for 3–4 h at 4 °C. The immunoprecipitates were then collected and washed five times with the lysis buffer before immunoblot analysis.

**Protein purification and size-exclusion chromatography.** The plasmids expressing hexahistidine (His)-tagged EPRS (amino acids 1–732, amino acids 1–196, and amino acids 1–168), His-tagged PCBP2 (amino acids 11–82 and amino acids 168–279), GST-fused PCBP2 (amino acids 11–82), and GST-fused MAVS (amino acids 460–540) proteins were transformed into *Escherichia coli* BL21-CodonPlus (DE3)-RIPL cells, and expression was induced by treatment with 0.5 mM IPTG at 18 °C for 18 h. The harvested cells were suspended in Buffer A (50 mM Tris-HCl, pH 7.5, and 150 mM NaCl) and lysed by sonication on ice. Cell lysates were centrifuged at 25,000 *g* at 4 °C for 1 h. The supernatants containing the His-tagged EPRS domains and the PCBP2 domains were loaded onto a Ni-NTA agarose column, washed extensively with Buffer A, and eluted with 250 mM imidazole. Supernatants containing GST-fused PCBP2 or MAVS domains were loaded onto a Glutathione Sepharose 4B column, washed with Buffer A, and eluted with 10 mM reduced glutathione. The purified proteins were then dialyzed against Buffer A and stored at −80 °C until use. Purified EPRS (amino acids 1–732) was examined by size-exclusion chromatography using a Superdex 200 10/300 GL column at 4 °C. Alcohol dehydrogenase (150 kDa) and albumin (66 kDa) were used as molecular weight standards. All eluted proteins were analyzed by SDS-PAGE, followed by staining with Coomassie Brilliant Blue.

***In vitro* precipitation assays.** Purified His-tagged EPRS domains (10 μM) and the GST-fused PCBP2 domain (20 μM) were mixed in binding buffer (50 mM Tris-HCl, pH 7.5, and 300 mM NaCl). In addition, purified GST-fused MAVS (10 μM) was mixed with the His-tagged PCBP2 domains (5 μM) in the binding buffer. These protein mixtures were then incubated with 50 μl of Ni-NTA agarose beads for 1 h at 4 °C. After washing with wash buffer (50 mM Tris-HCl, pH 7.5, 300 mM NaCl, and 10 mM imidazole), the bound proteins were eluted with elution buffer (50 mM Tris-HCl, pH 7.5, 300 mM NaCl, and 250 mM imidazole). Samples were loaded onto 4–12% SDS-PAGE gels and protein bands were visualized by Coomassie Blue staining.

**Histological analysis.** Brain samples were fixed in 4% paraformaldehyde, embedded in paraffin, and cut into 4-μm-thick sections. The sections were then deparaffinized with xylene and stained with hematoxylin-eosin. To detect VSV, brain sections were deparaffinized with xylene and subjected to antigen retrieval by microwaving in citrate buffer (pH 6.5). After staining with a VSV-G antibody (rabbit, 1:200), the sections were incubated with Alexa488-conjugated anti-rabbit IgG (1:250), followed by DAPI. Fluorescence images were captured with a Nikon laser scanning confocal microscope (C2plus) and processed using NIS-Elements software (Nikon).

**Confocal microscopy.** HeLa cells were seeded into eight-well plates (Labtek). After virus infection for different times, cells were fixed in 4% paraformaldehyde at 25 °C for 20 min. To obtain a clear image of the MSC complex, cells were incubated with 25 μg/ml of digitonin on ice for 10 min[43]. After permeabilization with 100% methanol for 20 min at −20 °C, cells were blocked with 2% bovine serum albumin in phosphate buffered saline (PBS) at 25 °C for 1 h. Cells were then washed three times with PBS-T (PBS containing 0.05% Tween-20) and incubated with the appropriate primary antibodies overnight at 4 °C. After washing a further three times, cells were incubated for 1 h at 25 °C with the appropriate secondary antibody. Cells were then stained with DAPI at 25 °C for another 10 min, washed three times in PBS-T, and mounted in mounting solution. Images were acquired under a Nikon laser scanning confocal microscope (C2plus) and analyzed using NIS-Elements software. The co-localization index based on the Pearson's correlation coefficient was calculated using the software tools[44].

**Mass spectrometry to identify EPRS phosphorylation sites and interactomes.** HEK293T cells were transfected with the Strep-EPRS plasmid construct for 24 h, followed by PR8-GFP (MOI = 5) for 6 h. Infected cells were harvested in lysis buffer (20 mM Tris-HCl, pH 8.0, 150 mM NaCl, 0.5% NP-40, and 1 mM EDTA) containing protease inhibitor and phosphatase inhibitor cocktails (Roche) and incubated with Strep-Tactin Superflow high capacity resin (IBA) overnight at 4 °C. The resin was extensively washed five times with the lysis buffer and bound proteins were eluted with elution buffer (100 mM Tris-HCl, pH 8.0, 150 mM NaCl, 1 mM EDTA, and 2.5 mM desthiobiotin). The final eluted fractions were concentrated in Amicon Ultra-4 (10K MWCO) centrifugation devices (Millipore). The samples were then analyzed by SDS-PAGE and silver stained. Stained protein bands were cut out and subjected to in-gel tryptic digestion as previously described[45]. Tryptic peptides were recovered and injected into a reversed-phase Magic 18aq (5 μm, 200 Å, Michrom BioResources) column (15 cm × 75 μm, packed in-house) coupled to an Eksigent MDLC system. The peptides were eluted at a flow rate of 300 nL/min with a 40 min linear gradient of 5–40% acetonitrile in acidified water (0.1% formic acid). The HPLC system was coupled to an LTQ XL-Orbitrap mass spectrometer (Thermo Scientific). Survey full-scan MS spectra (300–2,000 m/z) were acquired, with a resolution of 100,000 for precursor selection and charge state determination. The source ionization parameters were as follows: spray voltage, 1.9 kV; capillary temperature, 250 °C. The MS/MS spectra for the ten most intense ions with a charge state ≥ 2 from the MS1 scan were acquired using the following options: isolation width, 2.0 m/z; normalized collision energy, 35%; and dynamic exclusion duration, 30 s. Raw data were searched using the SEQUEST algorithm in Proteome Discoverer 1.4 (Thermo Scientific) and with the MASCOT search engine (v. 2.3.01; Matrix Science). The human Uniprot database (released in 2013.07) was searched using the following parameters: full tryptic peptide cleavage specificity, two missed cleavages, fixed modification of carbamidomethyl cysteine (+57.021 Da), variable modifications of oxidized methionine (+15.995 Da), and phosphorylated serine, threonine, and tyrosine (+79.9799 Da).

***In vivo* and *in vitro* ubiquitination assay.** HEK293T cells were transfected with different combinations of MAVS-FLAG, Itch-V5, GST-PCBP2, and Strep-EPRS plasmids. After 24 h, the cells were treated with 10 μM MG-132 for 6 h before lysis with RIPA buffer and immunoprecipitation with anti-FLAG affinity gel at 4 °C for 6 h. To detect endogenous MAVS ubiquitination, cell lysates were incubated overnight with a MAVS-specific antibody, followed by incubation with protein A/G PLUS-agarose beads at 4 °C for 3 h. The immune complexes were washed extensively five times with lysis buffer and boiled in SDS sample buffer for 10 min. Ubiquitination was analyzed using anti-ubiquitin or anti-K48-ubiquitin. For the *in vitro* ubiquitination assay, Strep-MAVS,




doi:10.1038/ni.3542

Strep-PCBP2, and Strep-EPRS proteins were pulled down from the lysates of HEK293T cells transfected with each of the plasmids. The Itch-V5 protein was prepared by incubating lysates with an anti-V5, followed by incubation with protein A/G PLUS-agarose beads. The purified proteins were incubated at 37 °C for 1 h with ubiquitin, E1 and E2 from UbcH5b (Boston Biochem) in a reaction buffer containing $Mg^{2+}$-ATP. The reaction was terminated by boiling followed by the addition of SDS sample buffer containing 1 mM DTT for 10 min. Ubiquitination was detected with an anti-ubiquitin.

**Aminoacylation assay.** To confirm enzymatic activity, His-tagged WT ERS (amino acids 1–732) and its catalytic mutant (R201L/R395L/S434A/K435L) were overexpressed and purified as described above. An aminoacylation assay was carried out in a buffer containing 30 mM HEPES-KOH, pH 7.5, 100 mM KOAc, 10 mM $Mg(OAc)_2$, 5 mM ATP, 4 mg/ml yeast total tRNA (R5636, Sigma), and 51.1 Ci/mmol [$^3$H] glutamic acid (NET490250UC, Perkin-Elmer). Reactions were carried out at 37 °C for 5 min and initiated by addition of ERS or its mutant (0.25 μM). Aliquots (20 μl) were spotted onto Whatman filter papers (1005110, grade 5, Whatman) pre-wetted with 5% trichloroacetic acid (TCA). The papers were washed three times for 10 min with 5% cold TCA and once for 20 min with 100% cold ethanol. After drying, the papers were placed into vials (Wheaton 986644) containing 4 ml of the liquid scintillation cocktail (Ultima Gold, Perkin-Elmer). Radioactivity was then measured in a scintillation counter (Perkin-Elmer).

**Peptide design and synthesis.** The EPRS L1 (amino acids 168–196) was fused with cell-penetrating human immunodeficiency virus type 1 Tat peptide (amino acids 47–57, YGRKKRRQRRR). The fused peptides (Tat-Epep) were then synthesized and purified to >93% by reverse-phase HPLC (AbClon). The Tat-Epep sequence is YGRKKRRQRRR-GG-DVSTTKARVAPEKKQDVGKF VELPGAEMG. TAT harboring the YGRKKRRQRRR sequence was used as a control peptide. Lyophilized peptides were stored in desiccant at −80 °C and dissolved in PBS before use.

**Cytotoxicity assay.** HEK293T or RAW264.7 cells were seeded in 96-well plates (10,000 per well) before treatment with Tat-Epep (20–200 μM) for 0–24 h. Cytotoxicity was determined in a colorimetric assay using MTS [3-(4,5-dimethylthiazole-2-yl)-5-(carboxymethoxyphenyl)-2-(4-sulfophenyl)-2H-tetrazolium salt] (Promega). MTS (20 μl) was added to each well at 37 °C for 1 h. Optical density (at 490 nm) was recorded using an automated microplate reader (BioTek). Background absorbance (at 630 nm) was subtracted from each sample reading.

**Statistical analysis.** Statistical analysis was performed using Prism (Version 6.0, GraphPad Software). Data were analyzed using Student's unpaired *t* test, the log-rank test or the non-parametric Mann-Whitney test, as appropriate. Normality of data was assessed using the Kolmogorov-Smirnov test. Data are expressed as the mean ± s.d. unless stated otherwise and all experiments were repeated independently at least three times.


40. Rosen, B., Schick, J. & Wurst, W. Beyond knockouts: the International Knockout Mouse Consortium delivers modular and evolving tools for investigating mammalian genes. *Mamm. Genome* **26**, 456–466 (2015).
41. Pascua, P.N. *et al.* Virulence and transmissibility of H1N2 influenza virus in ferrets imply the continuing threat of triple-reassortant swine viruses. *Proc. Natl. Acad. Sci. USA* **109**, 15900–15905 (2012).
42. Kim, S.K. *et al.* A nineteen gene-based risk score classifier predicts prognosis of colorectal cancer patients. *Mol. Oncol.* **8**, 1653–1666 (2014).
43. Han, J.M. *et al.* Leucyl-tRNA synthetase is an intracellular leucine sensor for the mTORC1-signaling pathway. *Cell* **149**, 410–424 (2012).
44. French, A.P., Mills, S., Swarup, R., Bennett, M.J. & Pridmore, T.P. Colocalization of fluorescent markers in confocal microscope images of plant cells. *Nat. Protoc.* **3**, 619–628 (2008).
45. Kim, K. *et al.* Reinvestigation of aminoacyl-tRNA synthetase core complex by affinity purification-mass spectrometry reveals TARSL2 as a potential member of the complex. *PLoS One* **8**, e81734 (2013).